Article

Eco-Friendly Synthesis of ZnO for Efficient Photodegradation of Pharmaceutical Drug Removal by Photocatalysis

Sharda Pandey,* Anchal Srivastava, Poonam Rawat, Satendra Kumar Chauhan, Anant Ram, Vishnu Kumar Diwedi, Rajesh Kumar Shukla, and Navina Wadhwani

Read Online

ACCESS | Metrics & More | Article Recommendations | SI Supporting Information

ABSTRACT: In the present work, a comparative study on eco-friendly synthesis of zinc oxide (ZnO) sample 1 and sample 2 with 3.17 and 4.17 M NaOH, respectively, is reported. Sample 2 with 4.17 M NaOH is applied in the photocatalytic degradation of paracetamol (pure and raw both) using the ultraviolet (UV, 280−400 nm) and UV/H_2O_2 reaction systems. Pure paracetamol (PCM1) and raw paracetamol (PCM2) from tablets are used for photocatalytic degradation by photocatalysis. Our experimental evidence show that ZnO sample 2 was more active in the UV/H_2O_2 reaction system than under ultraviolet (UV, 280−400 nm) irradiation only in the photocatalytic degradation process. Field emission scanning electron microscopy (FE-SEM) confirms the homogeneous growth of a rod-like structure for sample 1 and brittle and randomly aggregated rod-like and wire-like nanostructures for sample 2. The peaks observed in the region around 440 to 900 cm^{-1} in the FTIR spectra for sample 1 and sample 2 annealed at 250 °C confirms the presence of ZnO bonds. UV absorption spectroscopy indicates a red shift in the absorption spectra due to the increase in the molar concentration of NaOH to 4.17 M for sample 2. In this study, the band gap values are found to be 3.33 and 3.01 eV for the synthesized ZnO sample 1 and sample 2, respectively, which are 40 and 360 meV less as compared to that of bulk ZnO (3.37 eV). The oxidation rate is increased in the UV/H_2O_2 reaction system, producing the highest rate for PCM1 drug removal with rate constant 9.7×10^{-3} min^{-1} and half-life 71.5 min. The kinetic study results for the removal of PCM1 and PCM2 show good results and follow the pseudo-first-order kinetic model with correlation coefficients 0.69556 and 0.90851, respectively, whereas PCM2 follows the pseudo-second-order kinetic model with correlation coefficient 0.9993. The experimental and calculated values of removal capacity (q_e) at equilibrium is found close to those of the pseudo-second order kinetic model for the removal of both the paracetamol forms PCM1 and PCM2 with the catalyst ZnO nanostructure. The photostability of ZnO sample 2 is also tested with a reusability test in photocatalytic degradation of paracetamol at least four times. The absence of a maxima peak at 243 of PCM1 in the UV/H_2O_2 reaction system indicates nearly 100% successful conversion of 20 ppm PCM1 by using synthesized catalyst ZnO sample 2. The comparative results of both reaction systems, i.e., UV and UV/H_2O_2, show that the hydroxyl radicals, as the active species, are responsible for major degradation of both paracetamol forms (PCM1 and PCM2).
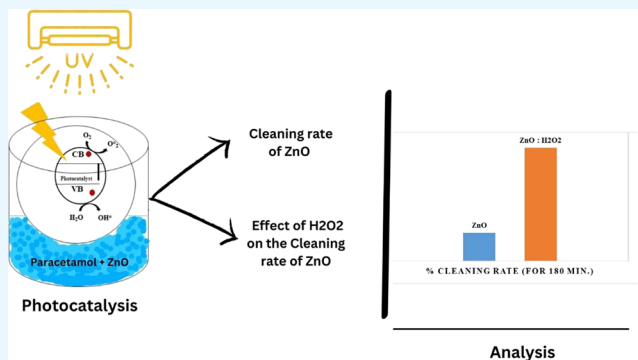
1. INTRODUCTION

Pharmaceuticals are a new group of micropollutants whose concentration in the water bodies increases due to the increase in the use of personal care products.[1−3] Drug manufacturing and improper disposal of unused medicines also add to the trace levels of pharmaceuticals in rivers, lakes, soil, and sometimes drinking water.[4−8] The occurrence of pharma drugs, prescription drugs, and medication over-the-counter drugs in wastewater and in the environment has been studied extensively in the USA, Canada, China, Spain, Greece, Netherlands, and South Africa, and their concentrations are found to be in the range of ng/L to μg/L.[9,10] An unregulated disposal of pharmaceutical wastes, dyes, and personal care products into our aquatic bodies degrades their quality

severely, which reduces the availability of clean water for the living species. Among all the wastes, paracetamol is an important drug due to its excessive use during Covid-19. From 2019, due to the outbreak of the Covid-19 pandemic, the use of paracetamol has increased manifold all over the world, which has led to a significant increase in the concentration of paracetamol in water bodies. This has resulted in a new class of

contaminants for water bodies. These compounds can have harmful effects, both acute and chronic, on natural flora and fauna.[11] In India, the prevailing concentration of paracetamol in water bodies is reported to be 4.6 μg/mL.[12] As the half-life of paracetamol is around 1–3 h, it therefore eventually enters the water body through urine or feces. As per the European technical guide on risk assessment, the prescribed no-effect concentration (PENC) of paracetamol in water bodies is 12.9 μg/L.[13] These reports are quite alarming for the healthy existence of aquatic life and living organisms. The concentration of paracetamol in water is expected to rise by several orders, and hence, in the present study, the concentration of paracetamol in stock solution is taken 20 mg/L, very high as compared to those in earlier works. The complete removal of pharmaceutical ingredients from water sources is a very difficult task. In recent times, advanced oxidation processes (AOPs) have led to interesting techniques for the removal of pharmaceuticals from water bodies. In this process, through oxidation and reduction, the water breaks into CO_2 and H_2O, which is less harmful to the environment.[14,15] Some most common oxidation-based processes are photolysis, UV radiation, photocatalysis, sonolysis, radiolysis, and ozonation.[16,17] Among these, photocatalysis has been used for the present study.

Extensive research has focused on photocatalytic degradation of paracetamol due to its injudicious use by using previously reported photocatalysts.[18,19] Among them, the most popular metal oxides used as catalysts are TiO_2, zinc oxide (ZnO), and SnO_2. These days, metal sulfide catalysts such as ZnS and CdS are also being used. Significant progress has been made in a number of scientific areas due to advancements in nanotechnology, particularly in the field of bioengineering materials. In the fight against diseases, such as bacterial infections and cancer, metallic and metal-oxide nanomaterials have been employed to identify important biomarkers whose measurement could lead to convincing clinical discovery. Nevertheless, progress is not unrestricted, and synthesizing this useful nanomaterial has some ecological and cultural implications, which affects the biomedical behavior of material. With the creative idea of using living organisms and biomolecules as unique reducing and capping specialists for the development of nanomaterial, green nanotechnology thus makes a strong claim as a potential solution to avoid the improvement of hazardous side effects and bother some reactions with various biological membranes.[20–22] Nowadays, surface-bound nanomaterials are also gaining momentum to many clean energy processes, including the production of lithium batteries and solar absorbers, solar-driven interface evaporation in desalination, photocatalytic reactions, wastewater treatment, and photolysis-based environmental remediation.[23] Here, ZnO nanostructures are chosen as a photocatalyst because of their versatile properties such as high surface area to volume ratio and synergistic electrical and thermal conductivities;[24,25] moreover, they are a wide-band-gap semiconductor of the II–VI group (E_g = 3.3 eV) and are therefore extensively used in optoelectronics, piezoelectronics, ultraviolet diodes, spintronics, photovoltaics, gas sensing, biosensing, sunscreens, drugs to rubber, ceramics, medicines, food, pigments, coatings, etc.[26,27] Fabrication of diodes using ZnO is attributable to its high excitation binding energy, 60 meV, at room temperature.[28] Because of their high surface energy, ZnO nanostructures (NSs) stimulate the production of reactive oxygen species (ROS), which are effective bacteria inhibitors and can

be used in biomedical applications. Furthermore, ZnO is gaining a lot of interest for environmental remediation applications such treatment of industrial wastewater due to its unique physical and chemical properties.[29] It is thought to be a promising photocatalyst that has the ability to degrade the majority of persistent organic pollutants, in the presence of UV light, which is only 3–5% of all sunlight.[30] ZnO is a nontoxic material, and if the traces of zinc will remain in the water after the treatment, it will not be affected badly to humans because zinc is an important element for living organisms. ZnO has the capability to oxidize the pollutant easily due to its wide band gap. Therefore, ZnO is a suitable option as a photocatalyst to oxidize pollutants from water. Numerous techniques, including sol–gel, homogeneous precipitation, mechanical milling, microwave synthesis, spray pyrolysis, thermal evaporation, and mechanochemical synthesis, can be used to synthesize ZnO, but these kinds of procedures usually involve the use of hazardous reducing agents and organic solvents, most of which are extremely reactive and detrimental to the environment. Therefore, eco-friendly synthesis routes have been employed for synthesizing ZnO NSs with the goal of minimizing the environmental impact. These environment-friendly nanomaterials have proven to be useful as biological specialists, offering substantial benefits over their traditionally synthesized reciprocals. Among these benefits are better cytocompatibility, organism clearance, and a modest synthetic approach that is both cost-effective and safe for the environment.[31] ZnO has garnered significant attention as a crucial nanomaterial for applications in bioengineering. By bringing about a synergistic impact in the properties of the crude material and the inherent elements of ZnO, it has successfully met eco-friendly techniques and inspired strong antibacterial, anticancer, and biosensing features. Various researchers such as Vasantharaj et al.[32] used biogreen-synthesized ZnO NPs for the degradation of methylene blue (MB) and malachite green (MG) and successfully removed 94 and 92% of MB and MG from water, respectively. Despotović et al.[33] tested the effect of ZnO nanoparticles in the removal of sulcotrione (SUL), clomazone (CLO), and amitriptyline. Sultana et al.[34] reported the use of ZnO NPs for the degradation of methyl orange (MO) successfully.

In the above literature survey, removal of pharmaceutical pollutants from water using ZnO is a subject of continuously ongoing studies. In the present paper, a simple and economical method is opted as an eco-friendly approach for the synthesis of ZnO samples at two different NaOH molar concentrations in aqueous medium and is used in the efficient photodegradation of pure and raw paracetamol removal by the photocatalysis method using ultraviolet (UV, 280–400 nm) and UV/H_2O_2 reaction medium. The results of the degradation patterns of both pure and raw paracetamol using synthesized ZnO with 4.17 M NaOH are compared with each other and also with the reported literatures. Therefore, the goal of this work is to investigate how the concentration of NaOH affects the physicochemical properties of ZnO synthesized via the sol–gel method and its photocatalytic degradation ability and how well it removes paracetamol in its pure and raw forms from water. A detailed discussion is addressed regarding the impact of hydroxyl ions on the reaction mechanism for the synthesis of the ZnO catalyst as well as the photocatalytic activity of the synthesized ZnO. The synthesized ZnO samples are characterized by the XRD powder diffraction technique, FE-SEM, FTIR, and UV–vis spectroscopy. The present work

**Scheme 1. Synthesis Route of ZnO NSs of Sample 1 and Sample 2**
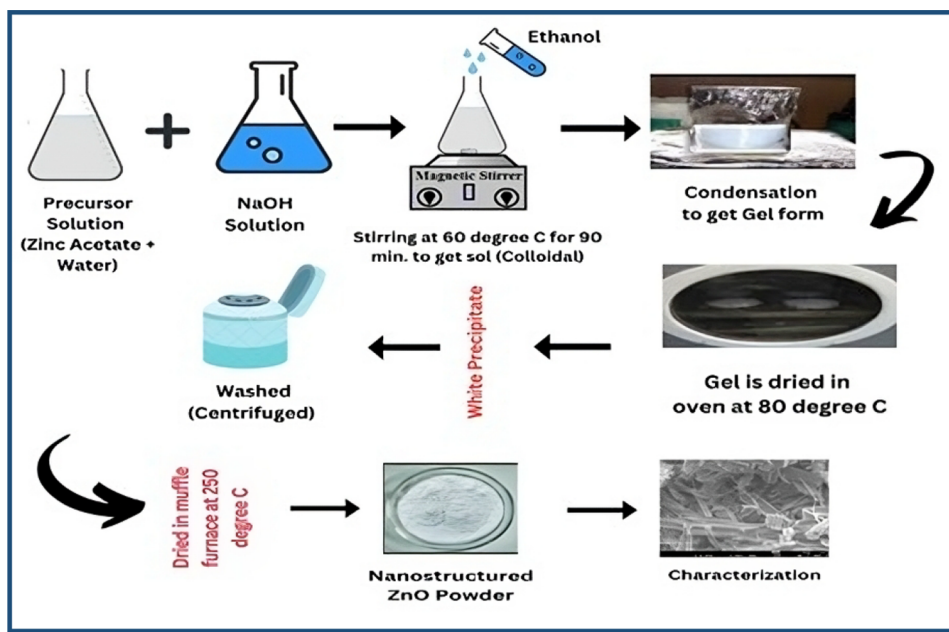
also bridges the gap in reporting the photocatalytic removal of commercially available paracetamol from tablet; mostly, researchers report the pure form of paracetamol. The detailed UV absorbance curve for the photocatalyzed samples is reported. The effect of environment-friendly reagent H_2O_2 on the enhancement of paracetamol removal in the presence of photocatalyst as-prepared ZnO NS and the reaction rates of photocatalytic degradation of PCM1 and PCM2 are also studied. The UV/H_2O_2 method is more effective for the photocatalytic degradation of organic pollutants. Therefore, our results of photocatalysis with the UV/H_2O_2 method do not exactly follow or fit well with the available theoretical approach. However, here, we wanted to check how much deviation there is in our results of photocatalysis in UV/H_2O_2 reaction system with the theoretical approach; we used the results of the photocatalytic degradation curves of the temporal decrease in absorbance in the UV/H_2O_2 reaction system to get the deviation.

2. MATERIALS AND METHODS

2.1. Chemicals and Reagents. Zinc acetate (99%, pure) and acetaminophen as PCM1 (99% pure) were purchased from Sigma-Aldrich. Ethyl alcohol (99% pure), diethanolamine (DEA) (99% pure), and sodium hydroxide flakes (99% pure) were purchased from Merck KGaA. Market-based paracetamol tablets were purchased from market. H_2O_2 (CAS No. 7722-84-1) was purchased from Thermo Fisher Scientific. Distilled water was collected from the Department of Chemistry, University of Lucknow. All of the purchased chemicals were used without further purification.

2.2. Method of Synthesis. *2.2.1. Eco-Friendly Synthesis of ZnO.* 0.1 M of zinc acetate precursor [M] solution was prepared in distilled water and two to three drops of DEA were added to stabilize the solution and magnetically stirred at 35 °C for 10 min to get a transparent solution. Then, the precursor solution was divided in two parts, named as solution 1 and solution 2. Two distinct molarities of NaOH solution 3.17 and 4.17 M were prepared. Then, 3.17 and 4.17 M

prepared NaOH solutions [OH] were added dropwise into precursor solution 1 (with [OH]/[M] ratio <40) and solution 2 (with [OH]/[M] ratio >40), respectively, and the pH is recorded as 10.49 and 11.83 of solution 1 and solution 2, respectively.[35] A turbidity was formed in the mixture. Afterward, 10 mL of ethyl alcohol was added in both solutions to clear the turbidity of the solution. The mixture was stirred at 60 °C for 90 min until the formation of gel. The gel was then dried at 80 °C for 22 h in an oven. A white precipitate obtained from both solutions was collected and washed five times with distilled water and ethanol to remove residuals. The resulting materials were named sample 1 and sample 2 and calcinated in a muffle furnace at 250 and 450 °C, for 3.5 h to yield powder ZnO NSs. The general reaction involved in the synthesis are given in the following:

$$Zn(CH_3COO)_2 2H_2O + 2NaOH$$
$$\rightarrow ZnO + 2CH_3COONa + H_2O \qquad (R1)$$
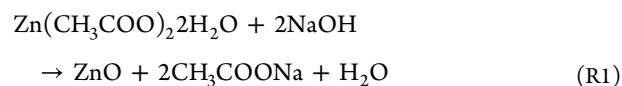
The systematic representation of the ZnO NSs is illustrated in Scheme 1. The formed compound was found stable at room temperature and obtained in good yield.

2.3. Characterization of the Photocatalyst. A structural analysis of the synthesized ZnO NSs was performed using XRD (model Rigaku Ultima IV) with Cu Kα (λ = 1.540598 Å). A morphological analysis was performed using a field emission scanning electron microscope (FE-SEM, JEOL, model JSM-7610F) (BSIP, Lucknow). The FTIR spectra were recorded in the range of 400 to 4000 cm^{-1} using an FTIR spectrophotometer (Shimadzu, IRAffinity-1S CE) with 30 scans and a 4 cm^{-1} resolution. Ultraviolet−visible near-infrared (UV−vis−NIR) spectroscopy (Model Jasco, V670) was used to record the absorption spectra, which were further used to determine the light harvesting capability of the synthesized ZnO photocatalysts. Using the Tauc equation, the band gap energy of the as-synthesized photocatalyst was then determined from the absorbance data. The as-obtained band gap energy determines the photocatalytic ability of the as-

synthesized ZnO photocatalyst. The lower the band gap, the better the photocatalytic efficiency of the as-synthesized ZnO photocatalyst. Using Agilent 6420 Triple Quadrupole MS equipment (CDRI, Lucknow), the mass spectra (MS) of the resultant intermediates were identified. All of the measurements were done at room temperature (300 K).

2.4. Experimental Method of Photocatalysis. The degradation of paracetamol ($C_8H_9NO_2$) was studied in two forms: (i) PCM1—pure paracetamol known as acetaminophen (Sigma-Aldrich) and (ii) PCM2—market-based paracetamol tablets, which include acetaminophen, microcrystalline cellulose, lactose, talcum powder, magnesium stearate, and starch. All the measurements of paracetamol degradation of PCM1 and PCM 2 were studied using sample 2 annealed at 250 °C.

An experiment on photocatalytic degradation was performed in a 150 mL borosilicate glass beaker fitted with a magnetic stirrer and a UV light source (280−400 nm), which were placed directly above the beaker at a 15 cm distance from the sample, as shown in Figure S2. The intensity of the UV light that reaches the reactor is measured using a digital lux meter (model: LX-1010B) and analyzed to be 2.75×10^{-5} Einstein s^{-1} (mol photons per second). A 20 ppm stock solution of PCM1 for which 2 mg of PCM1 is dissolved in 100 mL of distilled water is prepared. The solution is magnetically stirred for 10 min, and 4 mL of solution is taken out to record the UV absorption spectra. This will give the characteristic absorbance λ_{max} value for the pollutant. Furthermore, 50 mg/L ZnO sample 2 photocatalyst is added to the stock solution mentioned above and suspension is then allowed to aerate in the dark for 30 min to achieve an equilibrium between the catalyst and the pollutant paracetamol by adsorption−desorption. Afterward, 4 mL of solution is taken out and centrifuged to record the UV absorbance spectra of the supernatant for the 0 min analysis of degradation (no exposure of light). The beaker is now exposed to UV light irradiation for a definite duration. At certain times, aliquots of the paracetamol solutions were collected and centrifuged to extract the catalyst residues. Afterward, the absorbance was measured using a UV−vis spectrophotometer at 243 nm in the supernatant to determine how much paracetamol has been degraded. All these experiments were carried out in a wooden box in a dark room to avoid unwanted exposure to light.

The degradation of acetaminophen, PCM1, is measured by a decrease in the absorbance of the supernatant. A gradual change in the concentration of PCM1 with the time of exposure is observed. The change in absorbance value with respect to the time of exposure at a characteristic wavelength of 243 nm is used to determine the % paracetamol degradation Δ in water or percentage removal of paracetamol from water or percentage cleaning. It is given by eq 1:

$$\Delta = \frac{C_0 - C}{C_0} \times 100 = \frac{A_0 - A}{A_0} \times 100 \qquad (1)$$

where C_0 is the initial concentration of PCM1, C is the concentration of PCM1 after irradiation time t, and A_0 and A are the initial absorbance and that at a specified time of exposure, respectively.

To achieve an acceleration of oxidation and more rapid removal of PCM1 from water, the rate of reaction k has to be increased. For this, 3 mL of H_2O_2 was added, and the photocatalysis experiment was performed. Similar steps were also performed for the PCM2 degradation process. In order to

evaluate the role of photocatalyst in the paracetamol degradation process, an additional experiment involving the photodegradation of paracetamol (PCM1 and PCM2) was also performed in the presence of 3 mL of H_2O_2 and without the use of a catalyst. A reusability test was used to examine the stability of the photocatalyst. Following a single experiment cycle, the photocatalyst was centrifuged, cleaned with ethanol and deionized water, and allowed to air-dry for 24 h. Four cycles of the reusability test were performed.

3. RESULTS AND DISCUSSION

In this section, the experimental results, including structural and phase, morphological findings, and optical study along with functional group analysis, are discussed in detail.

3.1. X-ray Diffraction (XRD) Analysis. A structural study of the ZnO powder sample 1 and sample 2 in different molar concentrations of NaOH was performed using XRD for 2θ values ranging from 20 to 80° to confirm the formation of ZnO nanostructures and is shown in Figure 1. It is confirmed by
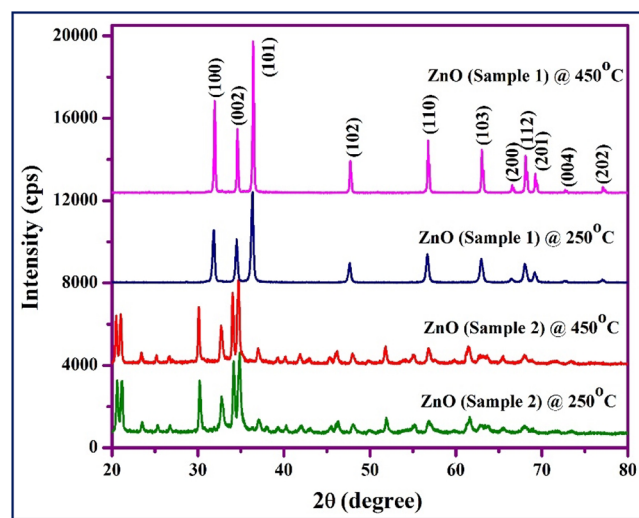

Figure 1. XRD patterns of synthesized ZnO samples 1 and sample 2.

XRD results that ZnO formation is influenced by the concentration of NaOH. Structural parameters of ZnO NS sample 1 and sample 2 using the XRD data are given in Table 1. The pH of the solution was measured using a pH meter (digital pH meter, model 111) before the suspension was put to heat at 60 °C and recorded as 10.49 and 11.83 when the concentrations of NaOH are 3.17 and 4.17 M for sample 1 and sample 2, respectively. The characteristic peaks of ZnO NS sample 1 synthesized from 3.17 M of NaOH and annealed at 450 °C are observed at 2θ = 31.86, 34.52, 36.34, 47.66, 56.68, 62.96, 66.48, 68.02, 69.12, 72.68, and 77.06°, due to diffraction from the planes along (100), (002), (101), (102), (110), (103), and (112), which indicates the hexagonal wurtzite NS of the ZnO powder sample. In contrast, the characteristic peaks of sample 2 annealed at 450 °C are observed at 2θ = 30.22, 32.80, 34.86, 46.01, 55.19, 61.54, and 67.81° due to diffraction from the planes along (100), (002), (101), (102), (110), (103), and (112), respectively. Thus, the synthesized ZnO samples are polycrystalline in nature. All the peaks are in good agreement with the standard JCPDS Card No. 005-0664.[36−38] The XRD spectra of ZnO sample 1 annealed at 250 and 450 °C indicate that ZnO was successfully formed without
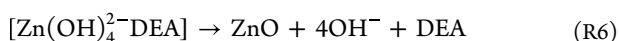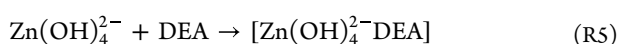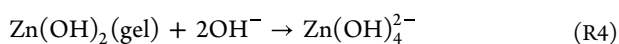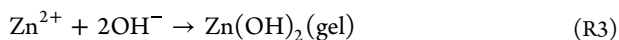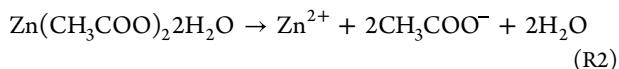
Table 1. Orientation Parameters along All the Reflection Peaks for Synthesized Samples

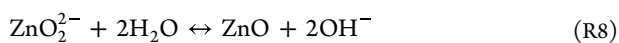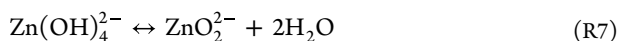|		orientation parameter $\gamma_{(hkl)}$										
samples		(100)	(002)	(101)	(102)	(110)	(103)	(200)	(112)	(201)	(004)	(202)
sample 1	250 °C	0.178	0.139	0.301	0.067	0.095	0.083	0.016	0.067	0.034	0.008	0.011
	450 °C	0.162	0.113	0.278	0.069	0.118	0.096	0.016	0.085	0.042	0.007	0.011
sample 2	250 °C	0.249	0.166	0.375	0.048	0.049	0.075		0.038			
	450 °C	0.254	0.162	0.365	0.057	0.045	0.076		0.043			

Table 2. Crystallite Size as Determined Using the DS Formula and WH Plot, Strain, Lattice Constants, and Dislocation Density Determined from XRD Data for ZnO Sample 1 and Sample 2

		t_{DS} (nm)					lattice constant			dislocation density $\delta \times (10^{14}$ line/m$^2)$		
sample		(100)	(002)	(101)	t_{WH} (nm)	micro strain (ε)	a (Å)	c (Å)	c/a	(100)	(002)	(101)
sample 1	250 °C	30.47	31.14	30.63	35.83	1.310×10^{-4}	3.24	5.19	1.601	10.76	10.30	10.66
	450 °C	51.33	55.11	54.31	48.14	1.175×10^{-3}	3.23	5.18	1.604	3.79	3.29	3.39
sample 2	250 °C	36.25	20.91	26.95	83.28	1.115×10^{-2}	3.42	5.46	1.597	7.61	22.87	13.77
	450 °C	48.39	27.69	30.82	214.24	6.240×10^{-3}	3.43	5.48	1.598	4.27	13.04	10.53

any impurity peaks. It is observed that ZnO NS sample 2 annealed at 250 and 450 °C shows a slight shift in peak toward a lower diffraction angle as compared with ZnO sample 1, which illustrates the consistent strain present in the crystallites of sample 2. The prominent peaks are along the (100), (002), and (101) planes, confirming the hexagonal wurtzite structure of ZnO sample 2 annealed at both 250 and 450 °C. Additionally, there is a broadening of the diffraction peaks, indicating a smaller crystallite size in the material. Rearranging the crystal plane in accordance with the conditions of synthesis can be seen by slight variations in peak intensity and broadening.[39] The group of dominant characteristics peaks are observed at $2\theta = 20.60$ and $21.17°$ along with minor peaks observed at $2\theta = 25.31$ and $26.72°$ originating due to the presence of zincate and sodium zincate in sample 2 synthesized from 4.17 M of NaOH.[40] The purity of ZnO sample 1 is 100.0% when the concentration of NaOH is 3.17 M. Meanwhile, this percentage is decreased to 79.71% for ZnO sample 2 annealed at 250 °C and 82.54% at 450 °C at the concentration of NaOH 4.17 M. The zinc acetate gives its dominant peak at 12.51°, which is not observed in synthesized samples 1 and 2, shown in Figure S1. Consequently, the following is a description of the proposed reaction mechanism for the formation of ZnO:

$$Zn(CH_3COO)_2 2H_2O \rightarrow Zn^{2+} + 2CH_3COO^- + 2H_2O \tag{R2}$$

$$Zn^{2+} + 2OH^- \rightarrow Zn(OH)_2(gel) \tag{R3}$$

$$Zn(OH)_2(gel) + 2OH^- \rightarrow Zn(OH)_4^{2-} \tag{R4}$$

$$Zn(OH)_4^{2-} + DEA \rightarrow [Zn(OH)_4^{2-}DEA] \tag{R5}$$

$$[Zn(OH)_4^{2-}DEA] \rightarrow ZnO + 4OH^- + DEA \tag{R6}$$

or,

$$Zn(OH)_4^{2-} \leftrightarrow ZnO_2^{2-} + 2H_2O \tag{R7}$$

$$ZnO_2^{2-} + 2H_2O \leftrightarrow ZnO + 2OH^- \tag{R8}$$

The growth of ZnO NSs is favored when the concentration of NaOH is less than 4.17 M. It seems that the primary ion of $Zn(OH)_4^{2-}$ cannot form at low hydroxyl ion (OH$^-$)

concentrations, leading to the creation of $Zn(OH)_2$. In this way, the given equation below illustrates how zinc hydroxide, in its unstable state, would finally reduce to a stable form of the ZnO nanoparticle.[41]

$$Zn(OH)_2 \rightarrow ZnO + 2H_2O \tag{R9}$$

However, if there are excessive amounts of hydroxyl ions present in addition to sodium ions, they will react with Zn or ZnO to produce zincate ions or sodium zincate ions.[42] The following is a description of the suggested mechanism:

$$ZnO + H_2O + 2NaOH \rightarrow Na_2Zn(OH)_4 \tag{R10}$$

$$ZnO + 2H_2O + 2NaOH \rightarrow Na_2Zn(OH)_4 + H_2 \tag{R11}$$
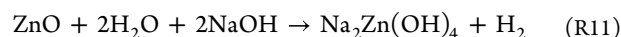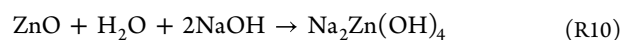
Equation 2 was used to determine the orientation parameter $\gamma_{(hkl)}$ along the plane (hkl)[43]:

$$\gamma_{(hkl)} = \frac{I_{(hkl)}}{\sum I_{(hkl)}} \tag{2}$$

The values of orientation parameters lie in the ranges of 0.008−0.301 and 0.007−0.278 for sample 1 annealed at 250 and 450 °C, respectively, whereas the ranges are 0.038−0.375 and 0.043−0.365 for sample 2 annealed at 250 and 450 °C, respectively, for all the reflection peaks, shown in Table 1. The major change in orientation parameters along the (002) and (101) planes for sample 1 indicates the uniform crystal growth along both polar and equatorial axes, with 3.17 M NaOH concentration, and for sample 2, it is along the (101) plane, indicating the growth along the equatorial axis, with 4.17 M NaOH concentration.

The crystallite size t_{DS} along different crystallographic planes is calculated by the well-known Scherrer formula and represented by eq 3:[43]

$$t_{DS} = \frac{0.9\lambda}{\beta \cos\theta} \tag{3}$$

where λ is the wavelength of X-ray employed and β (correct broadening) is the full width at half-maximum (FWHM) of the related X-ray peak in radians. The correct broadening (β) for a sample is calculated using relations 4a and eq 4b as follows:[44]
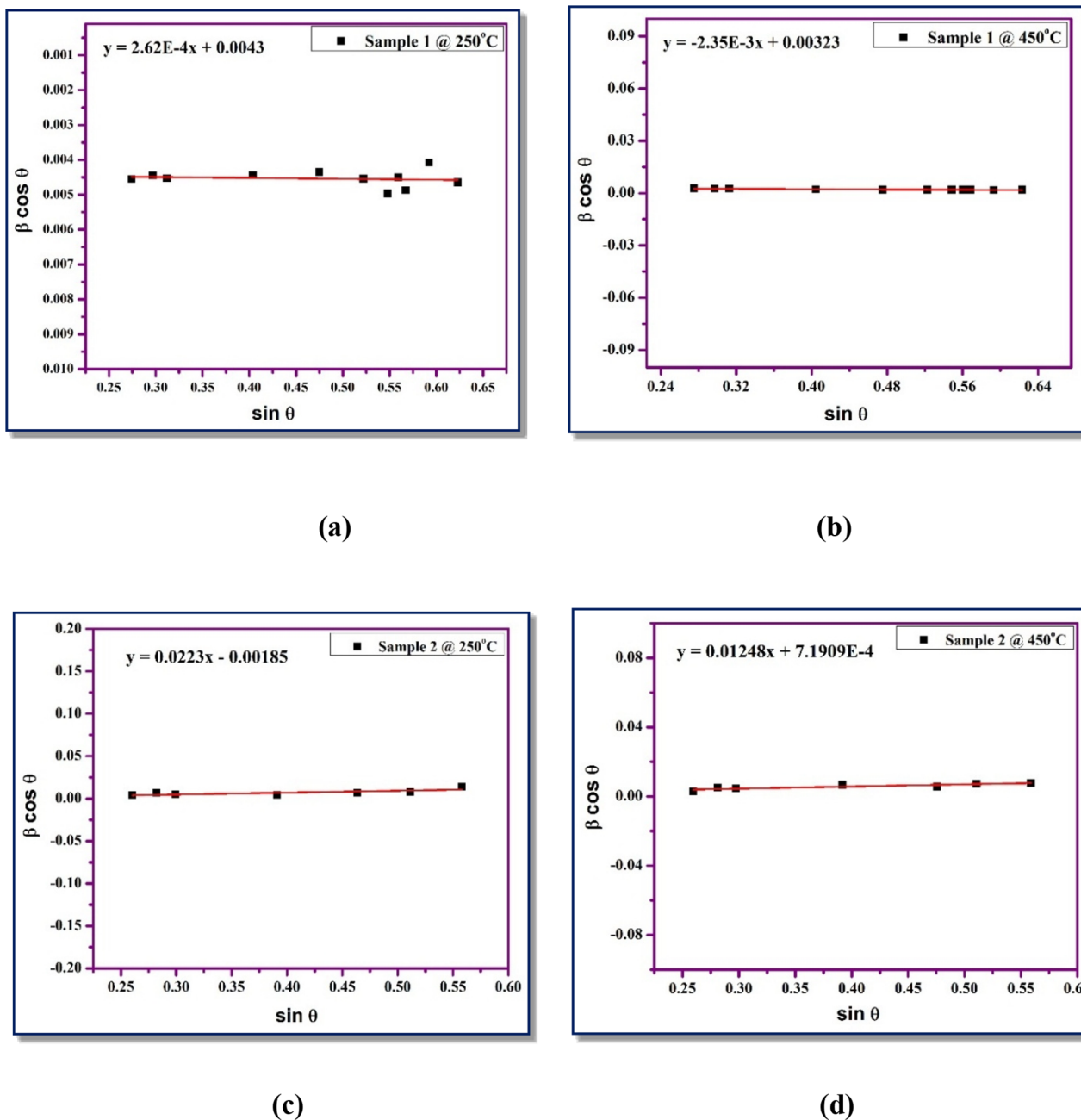
(a)

(b)

(c)

(d)

Figure 2. W–H plot of ZnO sample 1 (a, b) and sample 2 (c, d) annealed at 250 and 450 °C.

β = observed broadening − instrumental broadening

; (for Lorentzian)   (4a)

β = (observed broadening − instrumental broadening)$^{1/2}$

; (for Gaussian)   (4b)

In this work, a negligible order (10^{-5}) of instrumental broadening occurs only along the (202) plane in sample 1 and no kα_1 and kα_2 peak occur along the defined planes (Figure 1), except along the (202) plane. Therefore, the observed broadening is equal to the correct broadening, measured through the Gaussian distribution. The crystallite sizes of synthesized ZnO sample 1 and sample 2 annealed at 250 and 450 °C lie from 27.94 to 34.00, 51.33 to 74.73, 9.87 to 36.25, and 17.74 to 48.39 nm, respectively. The crystallite size along

three major planes of the hexagonal wurtzite structure of ZnO NSs annealed at 250 and 450 °C lie in the ranges of 20.91−36.25 and 30.47−31.14, respectively, as mentioned in Table 2, which shows that the annealing at 450 °C of ZnO NSs does not influence the phase of the material but the crystallinity and purity of the material have improved. Based on the above calculation, the range of variation in crystallite size of the sample along the defined planes has increased when the concentrations of NaOH increased from 3.17 to 4.17 M, and the sizes along the dominant plane (101) are 30.63, 54.31, 26.95, and 30.82 nm, respectively, for samples 1 and 2 both annealed at 250 and 450 °C, respectively, also mentioned in Table 2. The dispersity is particularly affected by the NaOH concentration, which causes the ZnO nanoparticles to agglomerate and hence increases the particle size.[39]

Stress and strain from XRD data are analyzed by using the Williamson−Hall (W−H) method. The crystallite size and lattice strain of synthesized ZnO sample 1 and sample 2 are determined in this study using the W−H method, as shown in Figure 2.

The trend line equations as obtained for ZnO sample 1 and sample 2 annealed at 250 and 450 °C are $y = 2.62 \times 10^{-4}x + 0.0043$; $y = -2.35 \times 10^{-3}x + 0.0032$ and $y = 0.0223x - 0.00185$; $y = 0.01248x + 7.1909 \times 10^{-4}$, respectively.

The standard trend line (eq 5) is[43,44]

$$\beta \cos \theta = \frac{C\lambda}{t_{WH}} + 2\varepsilon \sin \theta \tag{5}$$

used to calculate the synthesized materials' strain (ε) value and crystallite size (t_{WH}), where c is the correction factor, and its value is assumed to be 1. Table 2 lists the calculated strain and crystallite size data. As can be seen from Figure 2a,b, the strain for sample 1, annealed at 250 °C, is tensile in nature due to its positive slope, and it is compressive in nature for sample 1 annealed at 450 °C due to its negative slope. However, as can be seen from Figure 2c,d, the strain is tensile in nature for sample 2 annealed at 250 and 450 °C both because the slope is positive. On comparing the crystallite size obtained from the Debye−Scherrer formula, t_{DS}, and W−H method, t_{WH} are nearly close to each other for ZnO sample 1 annealed at both 250 and 450 °C, whereas ZnO sample 2 annealed at 250 and 450 °C shows discrepancy between the crystallite sizes obtained by the Scherrer method and the W−H method. This discrepancy arises due to incorporation of strain effect by the W−H method, which is not so in the case of the Scherrer method.

Table 2 shows that the as-prepared ZnO samples exhibit a decrease in the crystallite size as the NaOH concentration increases. This observation is corroborated by the samples' increasing strain values in relation to the NaOH concentration. The strain in the samples is inversely related with the crystallite size, as reported by several researchers,[39,45] and the above-mentioned data also clearly validates this. The change in lattice constants and charge-carrier gradient within the crystal lattice results in the change in bond length, which causes the strain in the samples. The strain may result in an overall decrease in crystallite size of the synthesized materials.[39] The variation in the crystallite size of the synthesized ZnO sample 1 and sample 2 (obtained by the W−H and Scherrer methods) with respect to the concentration of NaOH is shown in Table 2. Smaller crystallite sizes could be caused by two phenomena: (a) supersaturation and (b) NaOH reaction in the solution mixture. Supersaturation is important because it drives crystal nucleation and growth. At low supersaturation, crystals can grow faster than they nucleate, leading to larger crystal sizes; at higher supersaturation, crystal nucleation dominates crystal growth, leading to smaller crystals.[46] The obtained results are somewhat consistent with the observation that crystallite sizes decrease as supersaturation increases. An abrupt temperature gradient that led to rapid nucleation may have been produced during the synthesis by gradually adding NaOH to the zinc acetate solution. According to some theories, Na⁺ is drawn to the OH⁻ surrounding the nanocrystal and forms a virtual capping layer, which stops the nanocrystal from growing.[47] The result (eq R3) and (eq R4) need not always be $Zn(OH)^{2-}_4$; it might also be $Zn(OH)^+$, $Zn(OH)_2$, or $Zn(OH)^{3-}$, depending on a number of variables, including the concentration of OH⁻ and Zn^{2+} ions.[47] The size of the

nanocrystals fluctuates depending on the amounts of Na⁺ and OH⁻ ions, as the results for the samples show. The number of inherent and/or extrinsic flaws in the particles may have increased as a result of the strain that this size decrease may have placed on the crystal lattice.

The lattice constants a and c are determined using eq 6:[43,44]

$$\frac{1}{d^2_{hkl}} = \frac{4}{3}\left[\frac{h^2 + hk + k^2}{a^2}\right] + \frac{l^2}{c^2} \tag{6}$$

Here, d_{hkl} is the interplanar spacing for the plane (hkl) and is calculated using Bragg's law. The calculated values of the lattice constants a and c are reported in Table 2, which are larger than that of bulk ZnO. The values of lattice constants a and c decrease by 0.31, 0.62% and 0.29, 0.48% with respect to bulk ZnO, in sample 1, with 3.17 M NaOH and annealed at 250 and 450 °C, respectively. In contrast, the values of lattice constants a and c increase by 5.23, 5.54% and 4.89, 5.28% with respect to bulk ZnO, in sample 2, with 4.17 M NaOH and annealed at 250 and 450 °C, respectively. After annealing sample 1 at 450 °C, the value of lattice constants decreases uniformly by 10 meV, whereas sample 2 shows a nonuniform increase in the lattice constant values a and c by 10 and 20 meV, respectively, as can be seen in Table 2, which indicates that the expansion of the unit cell structure of the sample 2 lattice along the c axis is twice faster, leading to an increase in the surface area of as-prepared ZnO sample 2. The value of lattice constant 'a' increases by 180 and 200 meV with NaOH molar concentration 4.17 M in sample 2 annealed at 250 and 450 °C, respectively, as compared with the NaOH molar concentration 3.17 in sample 1. The value of lattice constant 'c' increases by 270 and 300 meV with 4.17 M NaOH in sample 2 as compared with the 3.17 M NaOH in sample 1 annealed at 250 and 450 °C. As can be seen from Table 2, the variation in the lattice constant c value is higher in sample 2 having 4.17 M NaOH; therefore, larger elongation takes place along the c axis as compared to the a and b axes in the synthesized ZnO NS for this NaOH to precursor molar ratio >40.

The ZnO bond length was calculated using eqs 7a and 7b:[48]

$$L = \sqrt{\frac{a^2}{3} + \left(\frac{1}{2} - u\right)^2 c^2} \tag{7a}$$

$$u = \frac{a^2}{3c^2} + 0.25 \tag{7b}$$

The values of bond length are 1.972, 1.966 and 3.507, 3.517 Å for ZnO samples 1 and 2 annealed at 250 and 450 °C, respectively, which indicates the compression of the ZnO sample 1 lattice and expansion of the ZnO sample 2 lattice. As the NaOH concentration increases to 4.17 M, the value of bond length of ZnO sample 2 increases by 90.18 and 78.89%, annealed at 250 and 450 °C, respectively, as compared to sample 1. The dislocation density parameter (δ) was used to examine the degree of defects present in the material, which is determined by applying Williamson and Smallman's equation 8):[49]

$$\delta = \frac{1}{t^2_{DS}} \tag{8}$$

The values of the lattice constants and the dislocation density (δ) are given in Table 2. The defect decreases in both samples 1 and 2 with the increase in annealing temperature,
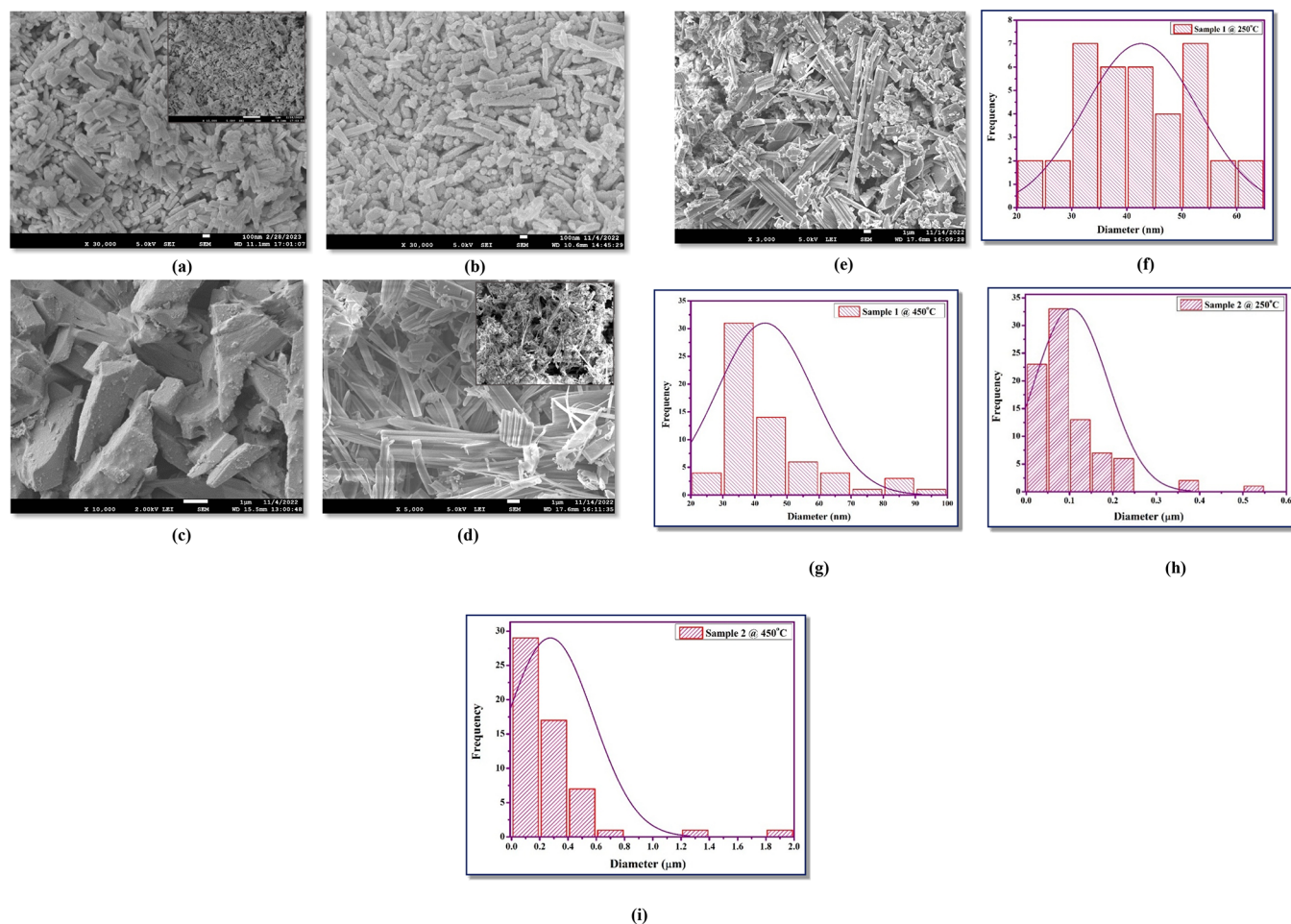
Figure 3. Surface morphology of ZnO nanostructure sample 1 (with [OH]/[M] ratio <40) annealed at (a) 250 °C and (b) 450 °C and for sample 2 (with [OH]/[M] ratio >40) annealed at (c) 80 °C, (d) 250 °C, and (e) 450 °C. The diameter distribution histograms of sample 1 (f, g) and sample 2 (h, i) annealed at 250 and 450 °C, respectively.

i.e., 450 °C. The value of δ is seen less along the axial plane (002) in ZnO sample 1 annealed at 250 and 450 °C, whereas in ZnO sample 2 annealed at 250 and 450 °C, it is seen less along the equatorial plane (100).

The value of strains ε_a and ε_c along the a axis and c axis are determined by eqs 9a and 9b:[37]

$$\varepsilon_a = \left(\frac{a - a_0}{a_0} \right) \tag{9a}$$

$$\varepsilon_c = \left(\frac{c - c_0}{c_0} \right) \tag{9b}$$

Here, a and c are the lattice constants and a_0 (=3.249) and c_0 (=5.205 Å) are the strain-free lattice constants for the bulk ZnO.[37] The calculated values of strains ε_a and ε_c for sample 1 are found to be 2.77×10^{-3} and -2.88×10^{-3} annealed at 250 °C and -5.85×10^{-3} and -4.80×10^{-3} annealed at 450 °C, respectively, whereas the values of strains ε_a and ε_c for sample 2 are found to be -5.26×10^{-2} and -4.89×10^{-2} annealed at 250 °C and -5.57×10^{-2} and -5.28×10^{-2} annealed at 450 °C, respectively. The positive value of strain indicates the tensile strain, and the negative value of strain indicates the compressive type of strain present along the a and c axes, which are also analyzed by the W−H method.

3.2. Surface Morphology of Synthesized ZnO. The chemical interactions between the concentrations of NaOH and the ZnO precursor determine the shape of the metal oxide (ZnO). Strong interactions primarily occur through ionic and covalent bonding between NaOH and ZnO. There are various NSs of ZnO as reported earlier such as nanosheets, nanorods, nanotubes, nanorings, nanowires, and nanobelts.[50,51] Zinc acetate was used as a precursor material, and its concentration was also an important factor in the formation of nanorods in addition to its nature. The FE-SEM image of synthesized ZnO powder samples is given in Figure 3. The FE-SEM image of ZnO sample 1 (Figure 3a,b) shows a rod-like structure, which indicates that the synthesized material shows better carrier transport facility, due to its smaller grain boundaries and surface defects.[50−53] Figure 3c shows the surface morphology of sample 2 after drying the sample at 80 °C. An annealing at 250 and 450 °C of sample 2 results in rod-like and wire-like structures, which are randomly dispersed throughout the sample and are nonhomogeneous (Figure 3d and e, respectively) made up of nanocrystallites, as revealed by XRD. Figure 3c−e also shows the agglomeration among particles with this NaOH to precursor molar ratio >40 of the as-prepared ZnO NS. The length and shapes of ZnO sample 1 are more symmetric (homogeneous) for [OH]/[M] ratio <40 of ZnO sample 1 in contrast with ZnO sample 2 having [OH]/ [M] ratio >40. The diameter of the NSs lies in the ranges of

23.08−61.54 and 40−544 nm for ZnO sample 1 and sample 2 annealed at 250 °C, respectively, as shown by the histogram in Figure 3f,h. However, the diameter lies in the ranges of 23.55−93.37 and 77−653 nm for ZnO sample 1 and sample 2 annealed at 450 °C, respectively, shown in the histograms of Figure 3g,i. The lengths of ZnO sample 2 are in a very irregular shape, annealed at 250 and 450 °C, as can be seen in Figure 3c−e, respectively. The diameter and its range for ZnO samples 1 and 2 annealed at 450 °C are comparatively large with respect to the samples annealed at 250 °C. This can be explained through the increase in temperature effect on annealing of both the samples 1 and 2, whereas increased molar concentration of NaOH present in comparison to the precursor is also a reason for the variation in diameter along with the temperature effect for sample 2. As in the case of sample 1, the low molar concentration of NaOH causes NSs to become smaller and their diameter variation reduces simultaneously. This demonstrates that a consistent and uniform growth process was enabled at the lower molar concentration of NaOH, i.e., below 4.17 M. The average diameters of ZnO NSs are 37.45, 27.35 and 74.76, 283.94 nm for sample 1 and sample 2 annealed at 250 and 450 °C, respectively. The average diameter of ZnO NSs is in close agreement with the values of crystallite size obtained from the XRD results (Table 2). The agglomeration among the particles is clearly illustrated in sample 2 with 4.17 M NaOH, as shown in the SEM image of ZnO NSs (Figure 3c−e). Therefore, agglomeration among the particles and their different shapes and sizes can be attributed to occur due to the surface tension enhanced by the higher NaOH molar ratio, which brings the particles together and are brittle.[46]

3.3. Vibrational Spectral Analysis. Figure 4 shows the FTIR spectra of synthesized ZnO samples 1 and 2 annealed at
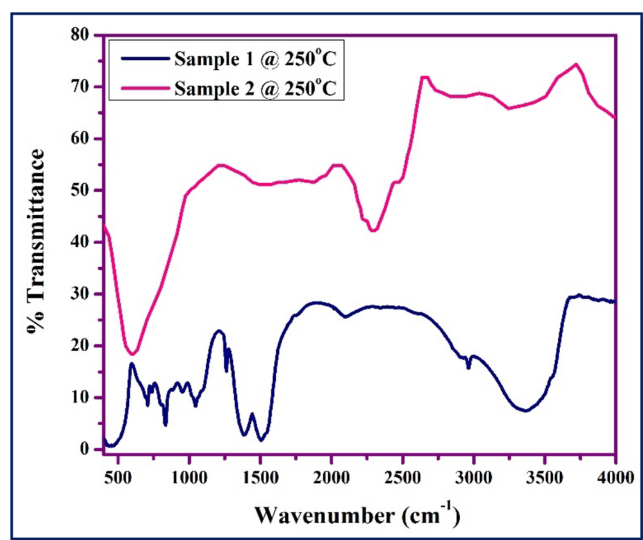

Figure 4. FTIR spectra of ZnO samples 1 and 2 annealed at 250 °C.

250 °C. A range of absorption peaks from 399 to 4000 cm^{-1} is seen in the spectra. The FTIR spectra for sample 1 and sample 2 annealed at 250 °C show absorption peaks in the region around 440 to 900 cm^{-1}, which are characteristic of the stretching mode of the Zn−O bond, indicating that ZnO is formed at this temperature, which is in agreement with the XRD results. The increase in intensity of the above-defined peaks is directly related with the increase in the number of

Zn−O bonds. Broad peaks at 3365.4 and 3248.6 cm^{-1} corresponds to the hydroxyl (−OH) group for the synthesized ZnO sample 1 and sample 2, respectively, annealed at 250 °C. The additional peaks found at 1510.6 and 1525.2 cm^{-1} correspond to the hydroxyl group (O−H) bending mode of water molecules for the synthesized ZnO sample 1 and sample 2, respectively. The bending vibration of the CO_2 mode is found at 2101.7 and 2292.8 cm^{-1} in sample 1 and sample 2, respectively. Weak peaks at 2960.4 and 2878.2 cm^{-1} correspond to the C−H stretching mode in sample 1 and sample 2 of synthesized ZnO, respectively.

3.4. UV Absorption Study. The UV−vis absorbance of the as-prepared ZnO NS is determined in the wavelength range 200−400 nm and is shown in Figure 5. As can be seen from Figure 5a and b, the resulting UV−vis spectra show a prominent excitonic absorption peak at 303 and 308 nm for synthesized samples 1 and 2 using 3.17 and 4.17 M of NaOH annealed at 250 °C, respectively, which is much less than bulk ZnO (373 nm) in the hexagonal phase of wurtzite. The single excitonic absorption peaks at 303 and 308 nm for synthesized ZnO samples 1 and 2, respectively, illustrate the remarkable optical characteristics and purity of the samples and also demonstrate good agreement with the XRD data (Figure 1). The absorption spectrum of the synthesized ZnO NS samples shows high absorbance in the UV region (below 400 nm) and the low absorbance spectrum in the visible region (above 400 nm). A red shift is observed due to the increase in the molar concentration of NaOH to 4.17 M for sample 2, which is due to the randomness and larger range of crystallite size from ∼10 to ∼36 nm for sample 2 along the defined planes obtained from XRD results and mentioned in Table 2, as compared with the synthesized ZnO sample 1 with 3.17 M NaOH. The optical band gap (E_g) of the synthesized ZnO NS samples 1 and 2 is obtained using Tauc's plot between $(\alpha h\nu)^2$ versus $h\nu$ and is given below in eq 10:[54]

$$(\alpha h\nu)^{1/n} = A(h\nu - E_g) \tag{10}$$

where A is the proportionality constant, α is the absorption coefficient, $h\nu$ is the photon energy incident on the sample, $n = 1/2$ represents the direct transition, and E_g represents the optical band gap energy. The value of the optical band gap was obtained by extrapolating the linear region of the curve to get an intercept on the energy axis, as shown in the inset curve of sample 1 (Figure 5a) and sample 2 (Figure 5b) of ZnO. In this study, the band gap values are found to be 3.33 and 3.01 eV for the synthesized ZnO sample 1 and sample 2, respectively, which are 40 and 360 meV less as compared to that of the bulk ZnO (3.37 eV). The decrease in band gap value relative to bulk ZnO indicates that the NaOH to precursor molar ratio <40 for sample 1 and the NaOH to precursor molar ratio >40 for sample 2 in the synthesized ZnO NS samples enhance the capability of the material to absorb the entire region of the UV−visible light spectrum for effectively utilizing the potential of the visible region of the light spectrum. On the basis of bandgap analysis, we expect that sample 2 with the NaOH to precursor molar ratio >40 could have better capability in the photocatalytic degradation of paracetamol as compared to sample 1 having a NaOH to precursor molar ratio <40. Compared to sample 2, sample 1 has a larger percentage of ZnO, which is responsible for its higher band gap of 3.17 NaOH concentration. The variations in E_g in the context of the decrease or increase in ZnO NSs' crystallite size are caused by
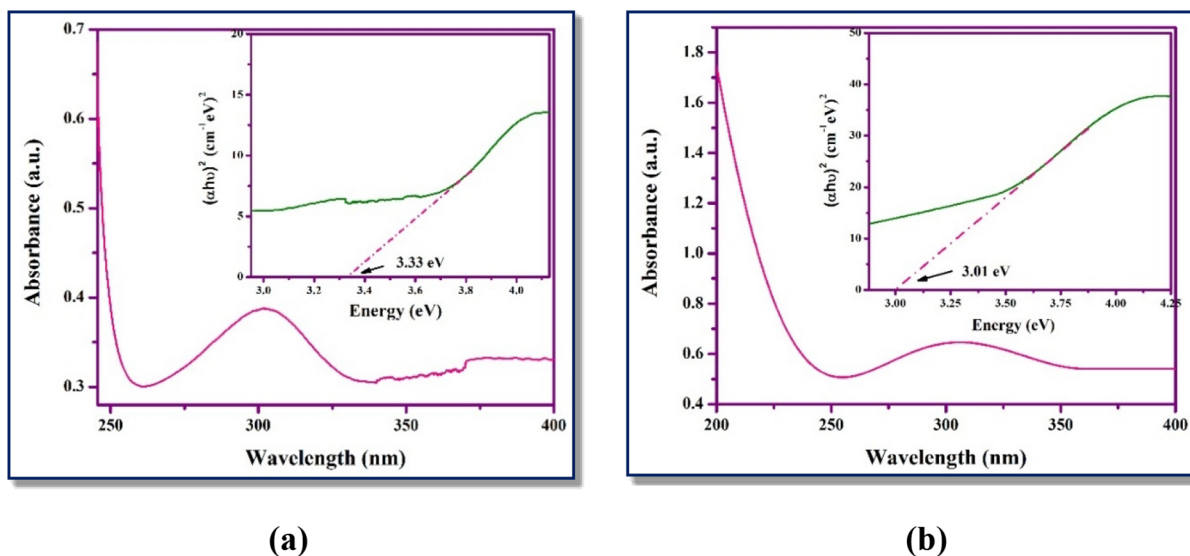
(a)

(b)

Figure 5. UV−vis absorption spectra of synthesized ZnO (photocatalyst) sample 1 (a) and sample 2 (b). The inset shows the Tauc plots of sample 1 and sample 2.

the optical confinement effect.[55] Adsorbed species and/or surface-related defects could possibly account for this behavior of E_g.[43,55] The energy band gap of ZnO is significantly influenced by its size, shape, and synthesis process. The higher annealing temperature leads to the lower band gap energy of ZnO. So, the low annealing temperature results in the high band gap energy of ZnO. ZnO is a visible light-sensitive photocatalyst. Therefore, the high band gap energy leads to lower absorption of visible light and, consequently, poor photocatalytic performance under visible light, which is not desirable.

3.5. Photocatalysis Analysis. The photocatalytic activity of metal-oxide semiconductors determines the ability of the photocatalysts (semiconductors) to oxidize the pollutant and break it into less harmful products, such as CO_2 and H_2O, as shown in Scheme 2. Here, the photocatalytic activity of the

Scheme 2. Diagram of Possible Mechanisms by Photocatalysis Using Zinc Oxide
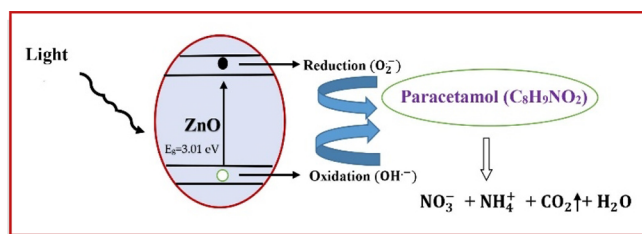
prepared ZnO NSs is used for the purpose of cleaning away paracetamol from water. Paracetamol being an analgesic and antipyretic medicine is regularly prescribed for not only humans but animals as well; therefore, mainly through fecal excretion, hospital waste, and pharmaceutical factories, para-cetamol finds its way to water bodies. The overuse of this medicine during Covid-19 increased its concentration in water bodies and placed the drug in a list of pollutants. However, addition of H_2O_2 is not essential for the photocatalytic removal of paracetamol, as shown in Figure S3.

The UV absorption spectra of PCM1 and PCM2 were studied by preparing their aqueous solution. Such spectra were also studied in the presence of ZnO as well as in the presence of bothZnO and H_2O_2. The aqueous solution of PCM1 is quite clear, as seen by unaided eyes. All the samples, i.e., PCM1 + ZnO, PCM2 + ZnO, PCM1+ ZnO + H_2O_2, and PCM2 + ZnO + H_2O_2, were subjected to centrifugation to obtain the supernatant. Figure 6 shows the absorbance of the
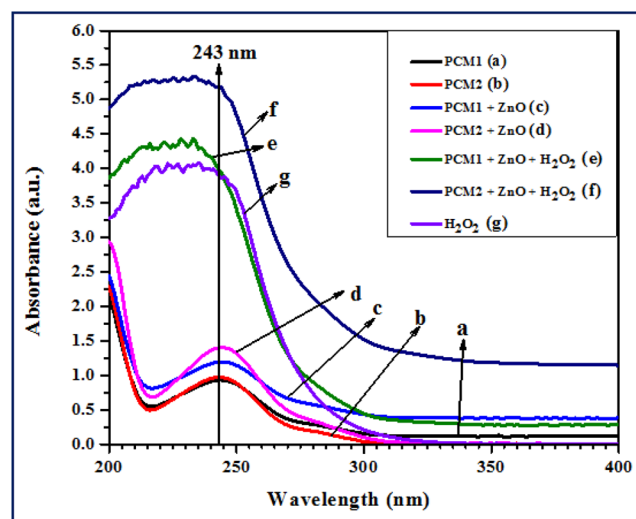
Figure 6. UV absorbance curves of supernatants of PCM1 and PCM2 and their combination with ZnO nanostructures and H_2O_2 prior to photocatalysis.

obtained supernatants in the wavelength region 200−400 nm for the normal incidence of light. Curves a, b, c, and d exhibit the characteristic absorption peak of paracetamol at 243 nm. Absorption at the wavelength 243 nm has also been reported in literature.[56,57] It should be recalled that the as-prepared ZnO NS sample 2 shows absorbance at 308 nm (Figure 5). Curve g shows the variation in absorption for H_2O_2 solution. The nature of curves e and f is dominated by the absorption behavior of H_2O_2 and shows increased absorption due to

addition of pollutants PCM1 and PCM2 respectively, as expected.

The UV absorbance curve of the supernatant was obtained from centrifuging for 10 min after photocatalysis of the pollutant PCM1 using catalyst ZnO NSs for different durations of UV exposure, as shown in Figure 7. Figure 7 corresponds to the photocatalysis of the sample PCM1 + ZnO for different time durations of exposure.

Figure 7. UV absorbance curve of supernatant obtained from centrifuging for 10 min after photocatalysis of the pollutant PCM1 using catalyst ZnO nanostructures for different durations of UV exposure.

Figures 8, 9, and 10 correspond to the samples PCM2 + ZnO, PCM1 + ZnO + H_2O_2, and PCM2 + ZnO + H_2O_2,
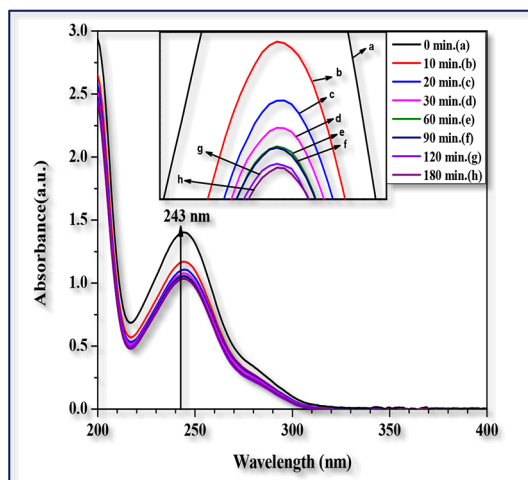
Figure 8. UV absorbance curve of supernatant obtained from centrifugation for 10 min after photocatalysis of the pollutant PCM2 using the catalyst ZnO nanostructure for different durations of UV exposure.
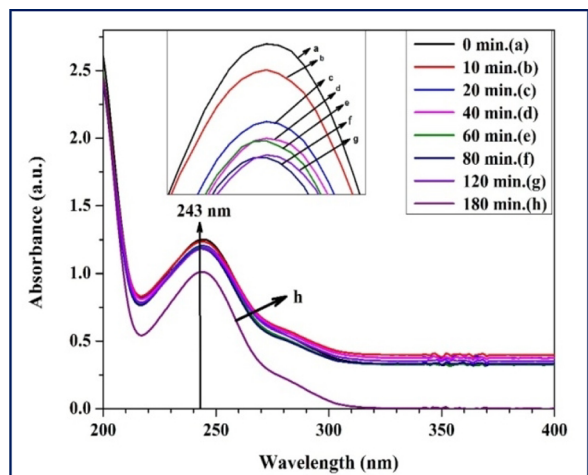
respectively. The absorbance at 243 nm goes on decreasing with an increase in time duration for all the samples (Figures 7 and 8).

For samples having H_2O_2 also, the absorption band is being displaced rather than disappearing with an increasing time duration for photocatalysis (Figures 9 and 10). Variation of absorbance, at characteristic wavelength 243 nm, with time for
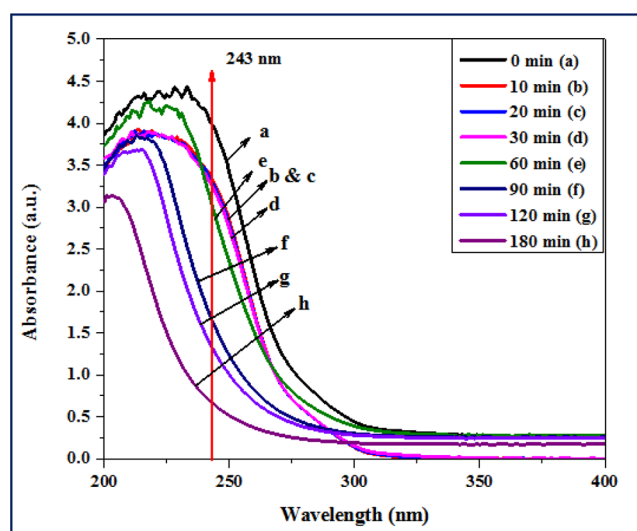
Figure 9. UV absorbance curve of supernatant obtained from a centrifuge for 10 min after photocatalysis of the pollutant PCM1 in the presence of the catalyst ZnO + H_2O_2.
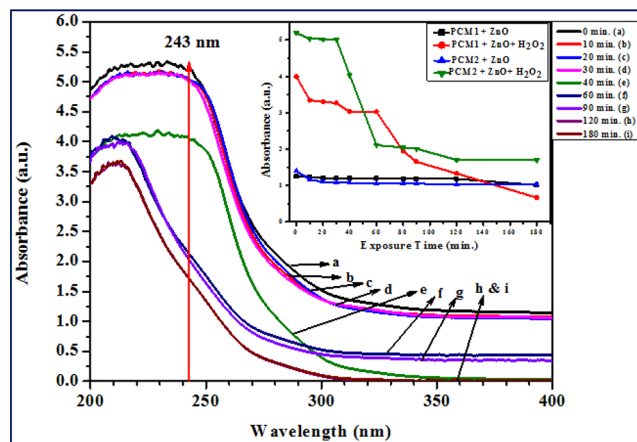
Figure 10. UV absorbance curve of supernatant obtained from centrifugation for 10 min after photocatalysis of pollutant PCM2 with ZnO + H_2O_2. The inset shows absorbance vs time curves for PCM1 and PCM2, derived from the main Figures 7−10, at the characteristic wavelength of 243 nm. Absorbance in the absence of H_2O_2 is also shown in the inset.

all the above-mentioned samples is shown in the inset of Figure 10. It can be seen that absorbance remains almost constant with time for the samples not having H_2O_2, and for the samples having H_2O_2, the absorbance reduces considerably with an increasing time duration of UV exposure. The temporal change in absorbance at 243 nm has been used for further studies of photocatalytic degradation of PCM1 and PCM2 with UV and UV/H_2O_2 reaction systems.

The curves in the inset of Figure 10 indicate that the photodegradation of paracetamol (PCM1 and PCM2) can be categorized as a first-order reaction.[58] Therefore, the reaction rate k is obtained from the given eq 11[58] and plotted in Figure 11.

$$\ln\frac{C_t}{C_0} = -kt$$

(11)
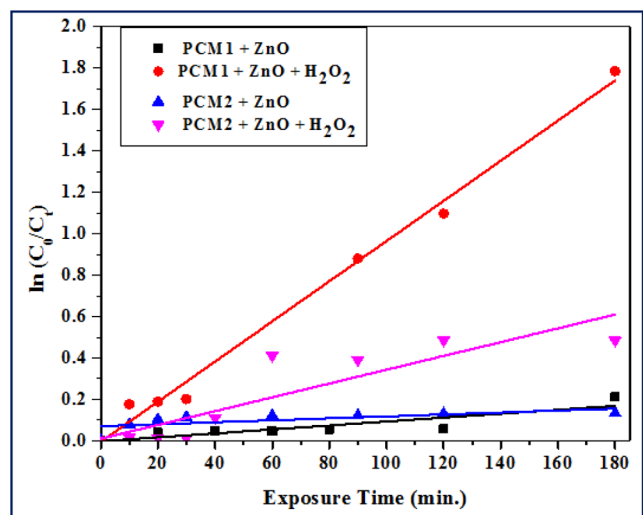
Figure 11. Kinetic reaction rates for the degradation of PCM1 and PCM2. The slopes determine the value of the first-order reaction rate constant k. The highest reaction rate constant is for PCM1 + ZnO+ H_2O_2.

The best linear fit is also presented, the slopes of which determine the values of k. The highest reaction rate constant is for PCM1 + ZnO + H_2O_2. The linear fits also indicate that the concentration c_t of the pollutant reduces with the passage of time under UV exposure. The half-life time $t_{1/2}$ of paracetamol, in this experiment, is calculated using eq 12[57]

$$t_{1/2} = \frac{\ln 2}{k} \tag{12}$$

and is mentioned in Table 5. It can be seen that for the present experiment, $t_{1/2}$ reduces drastically with addition of H_2O_2 in the presence of the catalyst ZnO NSs.

The percentage cleaning efficiency Δ calculated using eq 1 is plotted with respect to the exposure time duration in Figure 12. The cleaning efficiency increases considerably with the addition of H_2O_2 in the presence of the catalyst ZnO NSs. It is pertinent to mention here that H_2O_2 alone is not effective and
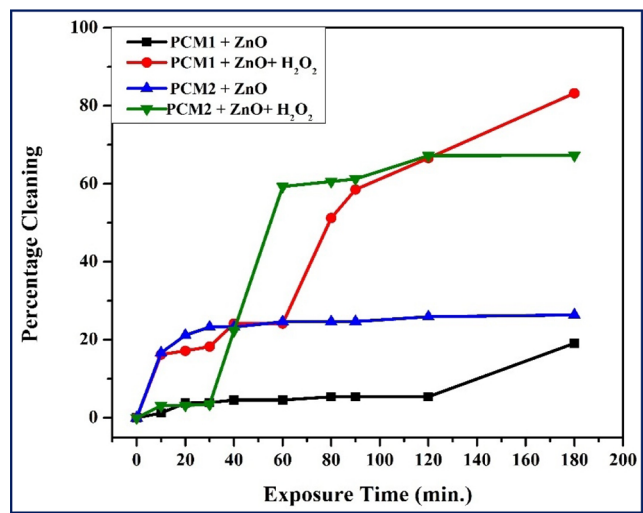

Figure 12. Percentage cleaning of water by photocatalytic degradation of PCM1 and PCM2 in the presence of catalyst ZnO nanostructures and that with the addition of H_2O_2.

no significant degradation occurs in the absence of catalyst ZnO, as inferred by our experiment and given in Figure S3.

The removal capacity q_t of the catalyst at time t is obtained using mass balance (eq 13):[59]

$$q_t = (C_0 - C_t)\frac{V}{W} \tag{13}$$

where C_0 and C_t are as defined earlier. C_0, V, and W are constants in the present condition. V (in liters) is the volume of the stock solution, and W (in g) is the amount of the as-prepared ZnO NSs, the catalyst. Equation 13 can be rearranged as eq 14:

$$q_t = C_0\left(1 - \frac{A_t}{A_0}\right)\frac{V}{W} \tag{14}$$

Figure 13 shows linear graphs for the removal capacity of ZnO NSs, determined using eq 14, for both PCM1 and PCM2. The addition of H_2O_2 shown in Figure 13b enhances the removal capacity drastically, more than three times, which is in conformation with the increase in reaction rate constant shown in Figure 11. The addition of H_2O_2 in the presence of catalyst ZnO NSs increases the supply of oxygen in the reaction, which generates more superoxide ions and hydroxyl radicals,[60] thereby enhancing the cleaning of water.

3.6. Possible Mechanism for Photocatalytic Degradation of Paracetamol. The schematic diagram of possible mechanisms by photocatalysis using ZnO with its band position representation is shown in Figure 14a, and various products formed during photocatalysis of paracetamol (pollutant) along with the final products are given in Figure 14b. The chemical structure of paracetamol is given in Table 3, and operating conditions of the photocatalysis experiment are shown in Table 4. The exposure of the photocatalyst ZnO NSs to UV radiation with energy equal to or greater than the band gap obtained, i.e., 3.01 eV, generates an electron hole pair as follows:

$$ZnO + h\nu \rightarrow ZnO + e^- + h^+ \tag{M1}$$

$$e^- + h^+ \rightarrow energy \tag{M2}$$
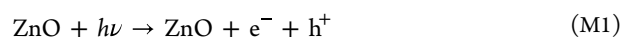
This newly created electron−hole pair migrates to the surface of the catalyst where the hole oxidizes a water molecule to form hydroxyl radicals and the electron reacts with the oxygen molecule to form super oxide radical ions.

$$h^+ + H_2O \rightarrow OH^- + H^+ \tag{M3}$$

$$h^+ + OH^- \rightarrow \dot{O}H \tag{M4}$$

$$e^- + O_2 \rightarrow O_2^- \tag{M5}$$

$$O_2^- + e^- \rightarrow O_2^{--} \tag{M6}$$

$$2O_2^- + 2H^+ \rightarrow H_2O_2 + O_2 \tag{M7}$$

$$O_2^- + H^+ \rightarrow HO_2^{\cdot} \tag{M8}$$

$$HO_2^{\cdot} + H^+ + e^- \rightarrow H_2O_2 \tag{M9}$$

$$H_2O_2 + h\nu \rightarrow 2\dot{O}H \tag{M10}$$

$$H_2O_2 + e^- \rightarrow \dot{O}H + OH^- \tag{M11}$$
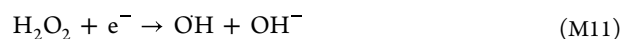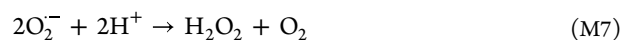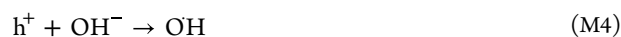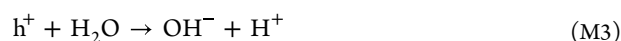
Using the following empirical formulas 15a and 15b, the valence band (VB) and conduction band (CB) potentials of
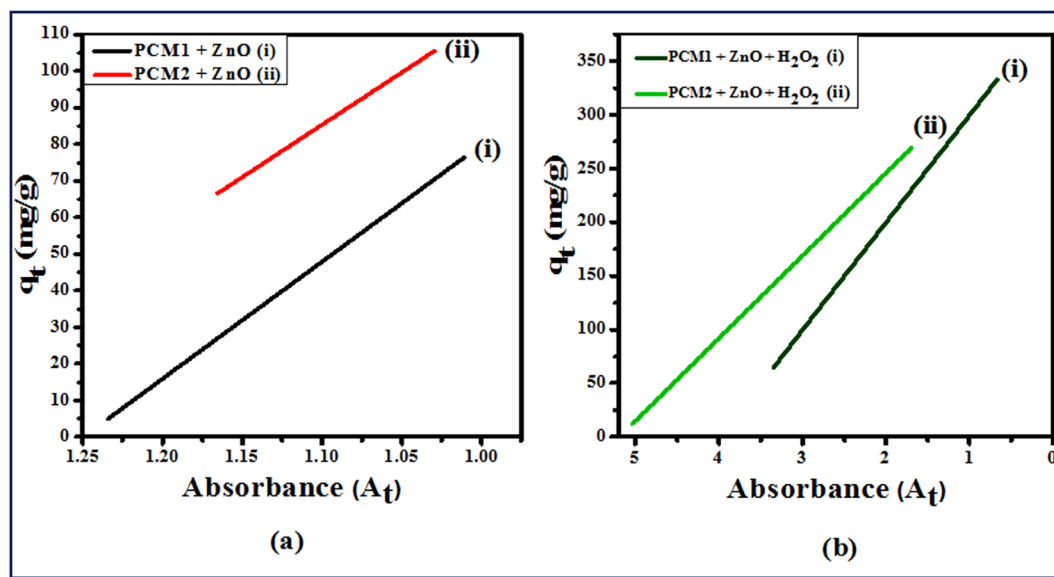
Figure 13. Removal capacity q_t, of catalyst ZnO nanostructures, vs absorbance at characteristic wavelength 243 nm for increasing exposure time without H_2O_2 (a) and with H_2O_2 (b).

synthesized ZnO sample 2 with 4.17 M NaOH and annealed at 250 °C with respect to the normal hydrogen electrode (NHE) are found to be 2.79 and −0.22 eV, respectively, as illustrated in Figure 14a:[54,61]

$$E_{VB} = X + 0.5E_g − E_c \tag{15a}$$

$$E_{CB} = E_{VB} − E_g \tag{15b}$$

where χ is the absolute value of the electronegativity of the semiconducting photocatalyst, E_{CB} is the conduction band potential, E_{VB} is the valence band potential, and E_C is the normal hydrogen electrode potential (about 4.5 eV). It has been found that ZnO has an electronegativity of 5.79 eV. According to the theoretical framework, ZnO sample 1 with 3.17 M NaOH and annealed at 250 °C has VB and CB potentials of 2.96 and −0.37 eV, respectively. The band gap energies of ZnO samples 1 and 2 are found to be 3.33 and 3.01 eV, respectively. With the absorption of the useful photon energy from UV light that has been irradiated, the e−h+ pairs are formed. Water molecules having an oxidation potential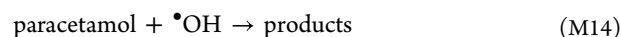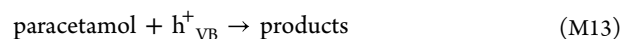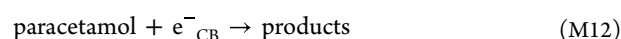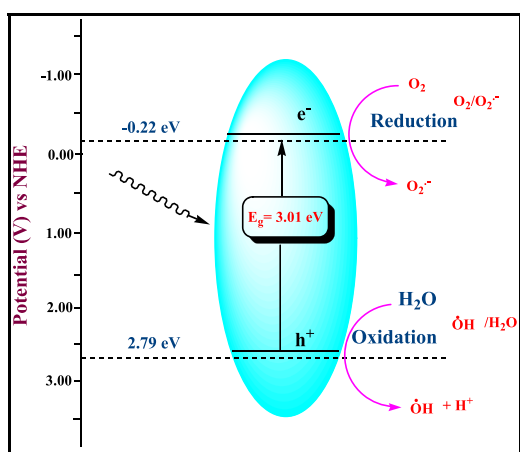 of E_0 (˙OH/H_2O) at 2.83 eV absorb this energetic hole from the low-lying edge of the valence band (2.79 eV). Figure 14b illustrates how effectively these produced ˙OH radicals play a crucial role in the breakdown of paracetamol. In a similar manner, the energetic electron absorption from air or the surroundings causes the production of superoxide radicals, which help in the breakdown of paracetamol and have a reduction potential of E_0 (O_2/$O_2^{˙-}$) at −0.18 eV.[62] The major role of ˙OH radicals over superoxide radicals has been already confirmed by performing the experiment in both UV and UV/H_2O_2 reaction systems, as shown in Figures 7−10. With the higher NaOH molar concentration 4.17 M, the stable small amount of zincate ions along with ZnO in sample 2 helps to generate a large amount of e− − h+ charges and also prevents their recombination, which leads to a huge amount of photoinduced charge for the effective and efficient photocatalytic degradation. The photocatalytic degradation experiment of paracetamol utilizing sample 2 annealed at 250 °C revealed that almost 83% of organic carbons were successfully

degraded in the UV/H_2O_2 reaction system in 180 min. The intermediates formed during the degradation reaction have been identified based on the λ_{max} value of potential organic components. Using ZnO sample 2 in the UV/H_2O_2 reaction system, the curves in Figures 9 and 10 at various temporal absorbance values show the presence of potential intermediates formed during the photocatalytic degradation of paracetamol.

During photocatalytic degradation of paracetamol, 13 intermediates have been identified in a decreasing order of molecular weight following the parent compound and are shown in Figure 14b. The structures of individual molecules, after the photocatalytic degradation of paracetamol, have been classified into four categories: (1) aromatic compounds, which are acetamide N-(3,4-hydroxyphenyl), acetamide N-(2,4-hydroxyphenyl), and hydroquinone; (2) five saturated carboxylic acids and one unsaturated carboxylic acid, which are malic, succinic, malonic, hydroxyl acetic acid, formic, and butanedioic; (3) nitrogen-containing straight chain compounds, including oxamic acid and acetamide; and (4) inorganic compounds, which are ammonium and nitrate. Using mass spectrometry, the relevant intermediate molecular weight was confirmed, and related mass spectra are provided in Figures S5, S6, S7, and S8. The produced OH radical affects hydroxylation of paracetamol by attaching itself with the aromatic ring with respect to the −OH position of paracetamol by replacing the NH group, eventually weakening the bonds thereby degrading the paracetamol. After the initial hydroxylation, further oxidation occurs, which produces carboxylic acids.[59,60] The active species e−, h+, O˙H, HO₂, and $O_2^{˙-}$ and H_2O_2 degrade the paracetamol in the presence of a ZnO catalyst. The hydroxyl radical (O˙H) is responsible for the major degradation of paracetamol (PCM1 and PCM2), as follows:

$$paracetamol + e^-_{CB} \rightarrow products \tag{M12}$$

$$paracetamol + h^+_{VB} \rightarrow products \tag{M13}$$

$$paracetamol + {}^{\bullet}OH \rightarrow products \tag{M14}$$

(a)

(b)

(c)
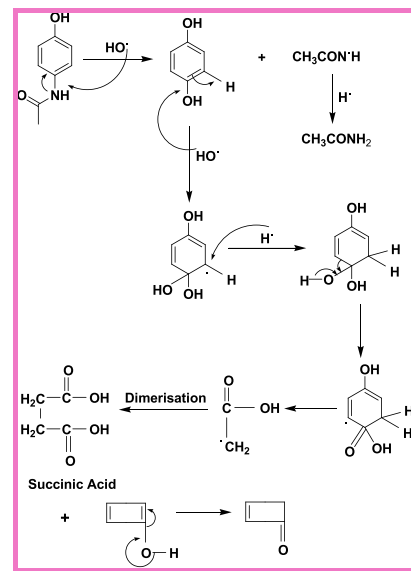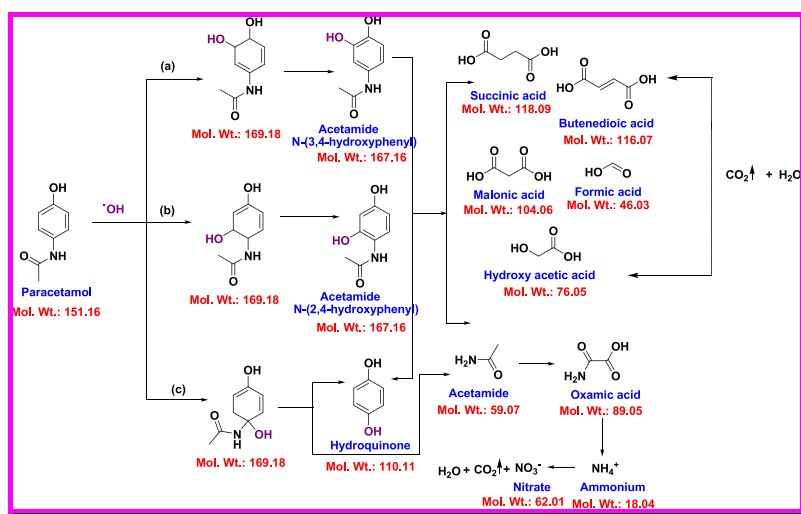
Figure 14. (a) Band position representation of ZnO sample 2 employed in the photocatalysis mechanism for paracetamol degradation. (b) Various possible intermediaries formed during photocatalysis of paracetamol (pollutant) along with final products and (c) generation of succinic acid by the hydroxylation of hydroquinone.

Table 3. Chemical Structure and Characteristics of Paracetamol

Chemical Structure	Synonyms	CAS no.	λ_{max} (nm)	Molecular Weight (g/mol)
	Paracetamol, Acetaminophen,	103-90--2	243	151.16

Table 4. Operating Conditions of the Photocatalysis Experiment

parameters	values
paracetamol initial concentration	20 mg/L
amount of catalyst ZnO	50 mg/L
UV bulb intensity	2.75×10^{-5} (Einstein/s)
temperature	300 K
pH	6.5

$$\text{paracetamol} + HO_2^{\bullet}/O_2^{\bullet-} \rightarrow \text{products} \tag{M15}$$

$$\text{paracetamol} + H_2O_2 \rightarrow \text{products} \tag{M16}$$

$$ZnO + h\nu + H_2O_2 \rightarrow e^-_{CB} + h^+_{VB} + 2^{\bullet}OH \tag{M17}$$

$$H_2O_2 + e^-_{CB} \rightarrow {}^{\bullet}OH + OH \tag{M18}$$
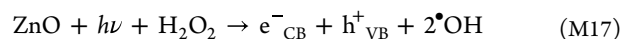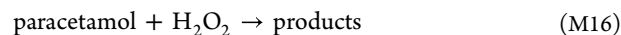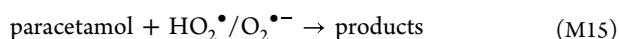
There is a large amount of production of hydroxyl radicals by the UV/H_2O_2 method. Therefore, the degradation reaction rate of paracetamol increases in the UV/H_2O_2 method; this indicates that the hydroxyl radicals play a major role in the degradation of paracetamol as compared with the superoxide radicals. This result has been confirmed by performing the photocatalytic degradation experiment of paracetamol in both

Table 5. Photocatalytic Response, i.e., Reaction Rate and Half-Life with Correlation Coefficient (R^2) for Paracetamol of Two Varieties

sr. no.	experimental ways	rate of constant (k) (min^{-1})	with standard error	half-life ($t_{1/2}$)(min.)	adj. R-square
1	PCM1 + ZnO	9.50029×10^{-4}	1.95619×10^{-4}	729.6	0.7634
2	PCM1 + ZnO + H$_2$O$_2$	0.0097	3.85858×10^{-4}	71.5	0.99059
3	PCM2 + ZnO	4.71582×10^{-4}	2.15685×10^{-4}	1469.8	0.35068
4	PCM2 + ZnO + H$_2$O$_2$	0.00333	6.53832×10^{-4}	208.2	0.75745

ways, i.e., with UV and with the UV/H$_2$O$_2$ method, and also by performing the scavenging activity test. The general view is that OH radicals generated by photolysis of H$_2$O$_2$ are the primary players in UV/H$_2$O$_2$ reaction system-based oxidations. In this study, isopropanol, an OH radical scavenger, was used, which slowed down the rate of paracetamol degradation reaction, as shown in Supplementary Figure S4, as compared with the results obtained from UV and UV/H$_2$O$_2$ reaction systems in the presence of catalyst ZnO. Paracetamol showed minimal to no deterioration when exposed to UV or H$_2$O$_2$, as seen in Figure S3. These results suggest that direct photolysis is not very important and that OH radicals really play a major role in the oxidative degradation of paracetamol and other phenolic compounds such as hydroquinone.

The λ_{max} of produced intermediaries such as acetamide N-(3,4-hydroxyphenyl), acetamide N-(2,4-hydroxyphenyl), hydroquinone, malic, succinic, malonic, hydroxyl acetic acid, formic, butanedioic, oxamic acid, and acetamide are 240, 238, 292, 209, 225, 290, 206, 205, 210, 200, and 205 nm, respectively. The absence of $\lambda_{max} > 210$ nm in the UV−vis spectra shows the maximum degradation of paracetamol except for some carboxylic acids. All the absorbance curves, before and after photocatalysis for a definite time durations, are shown in the Figures 6, 7, 8, 9, and 10. Mass spectrometry was also used to confirm the paracetamol degradation process and the associated intermediates, which are shown in Figures S5, S6, S7, and S8.

The initial photocatalytic oxidation of paracetamol corresponds to the formation of three aromatic compounds N-(3,4-dihydroxyphenyl) acetamide, N-(2,4-dihydroxyphenyl) acetamide, and hydroquinone, which showed a larger amount in comparison to other intermediates, as shown in the pathway reaction of Figure 14b, and is also confirmed by mass spectrometry as given in Figures S5−S8. Since these three components make up the foundation of paracetamol, their early presence is anticipated. According to routes a−c in Figure 14b, this suggests that the first step in the photocatalytic oxidation of paracetamol is the addition of ●OH onto the aromatic ring at ortho, meta, and para locations with regard to the −OH group of paracetamol. Thus, the early existence of these three aromatic components may be attributed to the hydroxylation of the (●OH interaction with) paracetamol. Under the plausible assumption that almost all of the acetamide that was first generated comes from the direct hydroxylation of paracetamol, one may argue that hydroxylation occurs to similar degrees at ortho and para positions only and meta hydroxylation is not very important, due to the presence of functional groups and their structural arrangement. Among the ortho and para positions of hydroxylation of these aromatic compounds, the ortho position of the − OH group of paracetamol may be preferred by the addition of ●OH to form N-(3,4-dihydroxyphenyl) acetamide. This may be caused by the adjacent −OH in the paracetamol benzene ring, which acts as a more potent electron donor group than the opposing

−NHCOCH$_3$. This makes the ortho position of the paracetamol structure more susceptible to attack by electrophilic hydroxyl radicals. Notably, further ●OH oxidation in N-(2,4-dihydroxyphenyl) and N-(3,4-dihydroxyphenyl) acetamide forms the corresponding trihydroxybenzenes, which would further release acetamide via hydroxylation. In PCM1 degradation reaction via ZnO+UV, the mass spectra show the dominant generation of hydroquinone for 180 min of the degradation process, whereas in PCM2 degradation in similar experimental ways for the 180 min of degradation duration, the mass spectra show the presence of higher amount of succinic acid. This shows that carboxylic acids such as succinic acid in the case of PCM2 are observed at 180 min, indicating that these three aromatic compounds listed as a, b, and c in Figure 14b serve as precursors for these carboxylic acids. Therefore, this difference in the degradation patterns of PCM1 and PCM2 in ZnO+UV indicates that their production processes may be comparable. The carboxylic acids produced in PCM2 degradation can be generated by cleaving aromatic rings and then oxidizing them further, as has been well-reported in published literature.[63,64] For example, successive ●OH oxidation of hydroquinone (identified in this study) in an aqueous environment results in the generation of p-benzoquinone, which is fairly unstable and tends to undergo ring rupture followed by further oxidation, forming carboxylic acids, as shown in the formation of succinic acid in Figure 14c. Succinic acid can then experience reaction with hydroxyl radicals, yielding malic acid, which is a precursor of malonic acid, which is identified in this study in a very low amount in mass spectra of PCM1 degradation in the UV/H$_2$O$_2$ reaction system.[64] The production of ammonium and nitrate, as shown in the pathway of Figure 14b, suggests that nitrogen in the aqueous phase can be readily transferred to volatile ammonia during the UV reaction system in the presence of ZnO for the photocatalytic breakdown of paracetamol.

As is shown in Figure 14b and also confirmed by the mass spectra in Figures S7 and S8 for PCM1 and PCM2 in the UV/H$_2$O$_2$ reaction system, initially within 10 min, the degradation of PCM2 is high due to the further hydroxylation of para position hydroxylation of the aromatic compound. The further oxidation by the hydroxyl radical of the generated intermediaries produces the carboxylic acids after 180 min of the degradation process of both paracetamol forms. The degradation of PCM2 as compared with PCM1 for the 180 min of photocatalytic degradation is slow and not consistent due to its stabilized synthesis conditions. Various ingredients used, which are mentioned in Section 2.4, are also responsible for this difference in the degradation pattern of raw and pure forms of paracetamol (Table 5).

3.7. Kinetic Studies of Paracetamol. The kinetic study is performed by using two models named the pseudo-first-order kinetic model and pseudo-second-order kinetic model. These models establish a relation between the photocatalysis mechanism and equilibrium concentration of pollutant with
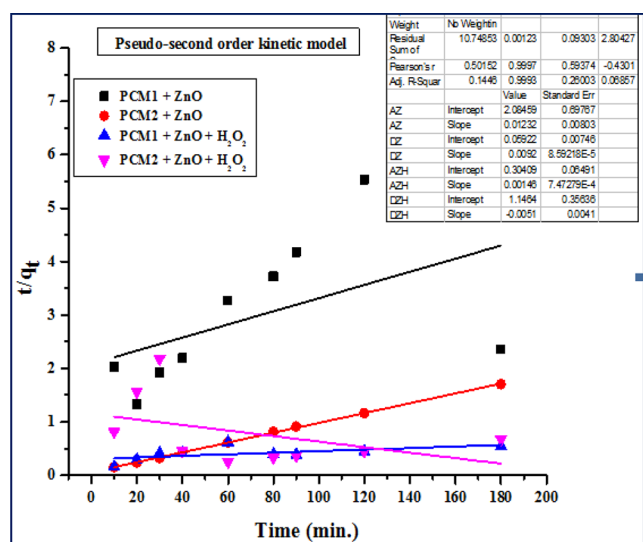
Table 6. Parameters Calculated from Two Kinetic Models for the Removal of PCM1 and PCM2 for Both the Experimental Types, i.e., with Catalyst ZnO Nanostructures (ZnO NSs) and ZnO Nanostructures: H$_2$O$_2$, in which the Effect of H$_2$O$_2$ Has Also Been Considered

catalyst	pollutants	model	type of experiment (catalyst and effect of H$_2$O$_2$)	parameters	calculated value	experimental value
ZnO NSs	PCM1 (raw)	pseudo-first-order	ZnO NSs	q_e (mg/g)	448.2585	76.5
			ZnO NSs: H$_2$O$_2$		1499.939	333
			ZnO NSs	k_1 (min^{-1})	−0.00024	
			ZnO NSs: H$_2$O$_2$		−0.00024	
			ZnO NSs	R^2	0.536	
			ZnO NSs: H$_2$O$_2$		0.69556	
		pseudo-second-order	ZnO NSs	q_e (mg/g)	81.16883	
			ZnO NSs: H$_2$O$_2$		684.9315	
			ZnO NSs	k_2 (min^{-1})	8.19703×10^{-5}	
			ZnO NSs: H$_2$O$_2$		2.96558×10^{-5}	
			ZnO NSs	R^2	0.1446	
			ZnO NSs: H$_2$O$_2$		0.26003	
	PCM2 (market-available tablets)	pseudo-first-order	ZnO NSs	q_e (mg/g)	67.78765	105.6
			ZnO NSs: H$_2$O$_2$		928.7411	269.2
			ZnO NSs	k_1 (min^{-1})	−0.00021	
			ZnO NSs:H$_2$O$_2$		−0.0003	
			ZnO NSs	R^2	0.86311	
			ZnO NSs: H$_2$O$_2$		0.90851	
		pseudo-second-order	ZnO NSs	q_e (mg/g)	108.6957	
			ZnO NSs: H$_2$O$_2$		−193.424	
			ZnO NSs	k_2 (min^{-1})	0.001502865	
			ZnO NSs: H$_2$O$_2$		1.20369×10^{-5}	
			ZnO NSs	R^2	0.9993	
			ZnO NSs: H$_2$O$_2$		0.06857	

time. Both kinetic models given by Ho and McKay[65,66] in linearized form are expressed in the following:

$$\ln(q_e - q_t) = \ln q_e - k_1 t \tag{16a}$$

$$\frac{t}{q_t} = \frac{1}{k_2 q_e^2} + \frac{t}{q_e} \tag{16b}$$

Here, eqs 16a and 16b are the mathematical expressions for the pseudo-first-order kinetic model and pseudo-second order kinetic model, respectively, q_e is the removal capacity at equilibrium, which indicates the amount of paracetamol mineralization at equilibrium, and k_1 and k_2 are the rate constants for pseudo-first-order and pseudo-second-order kinetic mineralization of paracetamol (in min^{-1}), respectively. The calculated parameters using these two models are given in Table 6. As shown in Figures 15 and 16, the correlation coefficients R^2 for the removal of PCM1 with the catalyst ZnO NS using the UV and UV/H$_2$O$_2$ methods are 0.53600 and 0.69556, respectively, for the pseudo-first-order and 0.14460 and 0.26003, respectively, for the pseudo-second order kinetic model. From the above results, it is evident that the degradation of PCM1 (raw) and PCM2 (pure) is governed by the pseudo-first-order model, which shows that physisorption phenomena take place in both the reaction system, i.e., UV and UV/H$_2$O$_2$. In raw form due to the impure structure, no consistent rate of degradation takes place compared to the pure form of paracetamol. This is why we have seen the huge difference in the value of R^2 for both the forms of paracetamol in the pseudo-first-order model under both UV and UV/H$_2$O$_2$ reaction systems, whereas, under the UV reaction system, the degradation of PCM2 strongly follows

Figure 15. Fitting curves based on the pseudo-first-order kinetic model in 20 ppm PCM1 and PCM2 mineralization with a catalyst ZnO nanostructure concentration of 50 mg/L for 180 min of photocatalysis. The effect of H$_2$O$_2$ on the mineralization reaction was also represented by up and down triangles.

the pseudo-second-order model, which indicates that the chemisorption phenomenon also plays an important role in the degradation of pure form and also controls the rate of degradation. This behavior of PCM2 is due to its stabilized structure, achieved by definite synthesis conditions. The R^2 value of the pseudo-second-order model for the UV reaction system indicates that the ingredients involved in the synthesis

Figure 16. Fitting curves based on the pseudo-second-order kinetic model in 20 ppm of PCM1 and PCM2 mineralization with the catalyst ZnO nanostructure concentration of 50 mg/L for 180 min of photocatalysis. The effect of H_2O_2 on the mineralization reaction has also been represented by up and down triangles.
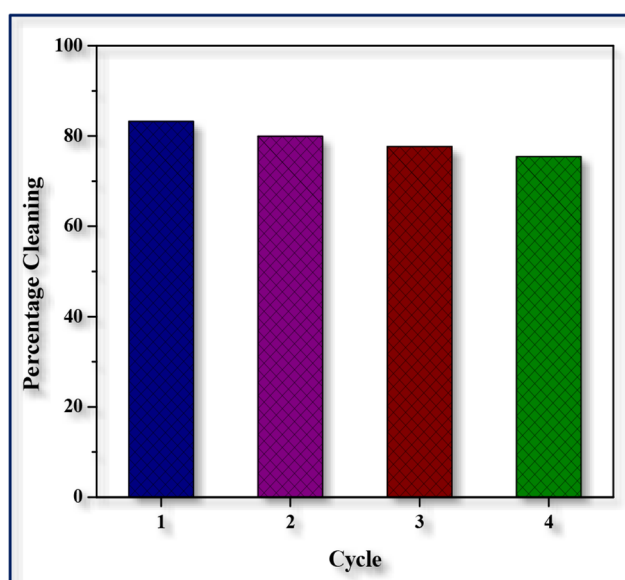

Figure 17. Percentage cleaning of water to determine the reusability of catalyst as-prepared ZnO nanostructures for four consecutive photocatalysis experiments using fresh solution of pollutant PCM1.

of pure form of paracetamol (PCM2) will probably form a strong bonding with the photocatalyst ZnO in the degradation process, which will certainly reduce the reusability of the photocatalyst. This work will be considered as a future study to check the difference in the reusability of photocatalyst involved in the raw and pure forms of paracetamol.

Similarly, R^2 for the removal of PCM2 with the catalyst ZnO NS using UV and UV/H_2O_2 methods are 0.86311 and 0.90851, respectively, for the pseudo-first-order and 0.9993 and 0.06857, respectively, for the pseudo-second-order kinetic model. Therefore, results show that the mineralization of paracetamol is in agreement with the pseudo-first-order model. However, the removal of PCM2 with catalyst ZnO NS (i) with UV is strongly dominated by the pseudo-second-order kinetic model, and (ii) that with UV/H_2O_2 strongly shows disagreement with the pseudo-second-order kinetic model.

The experimental and calculated values of q_e are close to the pseudo-second-order kinetic model for the removal of both the paracetamol forms with the catalyst ZnO NS, mentioned in Table 6, and Figure 17 shows the percentage cleaning of water to determine the reusability of the synthesized catalyst ZnO NS for four consecutive photocatalysis experiments using fresh solution of pollutant PCM1.

3.8. Quantum Yield for the Photocatalytic Degradation of Paracetamol. The quantum yield, also known as quantum efficiency, is determined by dividing the initial response rate ($r_{initial}$) by the input photon flux (Φ),[54,67] and the corresponding eq 17 is as follows:

$$QY = \frac{r_{initial}}{\Phi} = \frac{kC_0}{\Phi} \tag{17}$$

where C_0 (mol/L) is the initial concentration of paracetamol and k is the kinetic rate of degradation reaction. The values of k are 9.50×10^{-4} and 9.70×10^{-3} min^{-1} for PCM1 and 4.72×10^{-4} and 3.33×10^{-3} min^{-1} for PCM2 in both UV and UV/H_2O_2 reaction systems, respectively, as shown in Table 4. The initial concentration (C_0) of paracetamol is 1.323×10^{-4} mol/L. Therefore, the values of $r_{initial}$ are 0.126 and 1.283 μmol L^{-1}

min^{-1} for PCM1 and 0.063 and 0.441 μmol L^{-1} min^{-1} for PCM2 in the UV and UV/H_2O_2 reaction systems, respectively. Accordingly, it has been found that the resulting quantum efficiencies in the paracetamol degradation process are ~0.08 and 0.78% in the case of PCM1 and ~0.04 and 0.27% in the case of PCM2 for ZnO sample 2 under the UV and UV/H_2O_2 reaction systems, respectively.

3.9. Regeneration and Reusability Study. The potential of reuse of the as-prepared ZnO sample 2 for photocatalysis is tested by performing consecutive paracetamol degradation cycles with the same ZnO NSs that were used in the first cycle of photocatalysis. The UV exposure time is 180 min for each cycle. The collected sample of ZnO sample 2 from the first photocatalysis cycle is washed using distilled water three times in a very careful manner for eliminating the traces of remaining paracetamol. The washed ZnO NSs are dried in an oven to remove the moisture content present in it and to make it reusable for the next cycle. After each washing, the amount of collected sample of ZnO reduces, as determined by weighing. The recycle experiment was performed four times. The percentage cleaning after each cycle is approximately 83%, which implies that the photocatalytic degradation of more than 80% of paracetamol in the water sample has taken place. It is shown in a bar graph in Figure 17.

Comparison of the performance of synthesized ZnO NS sample 2 (photocatalyst) for the photocatalysis with previous studies is shown in Table 7. 83% removal of PCM1 for 20 ppm pollutant has been achieved by photocatalysis in the presence of the synthesized ZnO sample 2 and H_2O_2. A similar process in the case of the market-based PCM2 resulted in 67% removal of the pollutant after 180 min of exposure time. By earlier researchers, different semiconductor photocatalysts ZnO, TiO_2, and Fe_2O_3 and composites in nanoparticle and thin film forms have been explored for the degradation of paracetamol. To clearly justify the performance of ZnO sample 2 alone and along with H_2O_2 for degradation of paracetamol, the results obtained in our work have been compared with those reported in the literature.

Table 7. Comparison of Performance of Synthesized ZnO Nanostructures (Photocatalyst) for the Photocatalysis with Previous Studies

name of pollutant	type of catalysts	light source	experimental conditions	% removal/ exposure duration	references
PCM1 (raw paracetamol)	synthesized ZnO nanostructures (sol–gel), annealing at 250 °C	UV lamp (25 W) (280–400 nm)	[pollutant] = 20 ppm, [catalyst] = 50 mg/L, pH = 6.5, temperature = 27 °C	~22%; 180 min	our work
PCM1 (with H_2O_2) (raw paracetamol)	synthesized ZnO nanostructures (sol–gel), annealing at 250 °C	UV lamp (25 W) (280–400 nm)	[pollutant] = 20 ppm, [catalyst] = 50 mg/L, pH = 6.5, temperature = 27 °C	83%; 180 min	our work
PCM2 (market-based paracetamol)	synthesized ZnO nanostructures (sol–gel), annealing at 250 °C	UV lamp (25 W) (280–400 nm)	[pollutant] = 20 ppm, [catalyst] = 50 mg/L, pH = 6.5, temperature = 27 °C	~20%; 180 min	our work
PCM2 (market-based paracetamol) (with H_2O_2)	synthesized ZnO nanostructures (sol–gel), annealing at 250 °C	UV lamp (25 W) (280–400 nm)	[pollutant] = 20 ppm, [catalyst] = 50 mg/L, pH = 6.5, temperature = 27 °C	67.27%; 180 min	our work
paracetamol	synthesized ZnO (sol–gel), annealing at 500 °C	UV lamp (25 W) (315–400 nm)	[pollutant] = 15 ppm, [catalyst] = thin film, pH = 5.58–6.69, temperature = 25 °C	~14%; 240 min	Pronin et al.[56]
paracetamol	TiO_2	UV lamp (254 nm), intensity = 12.6 mW/cm²	[pollutant] = 4.0 mM/L, [catalyst] = 0.4 g/L, pH = 9.5, temperature = 26 °C	60%; 450 min	Yang et al.[63]
paracetamol	TiO_2	UV lamp (254 nm), Intensity = 12.6 mW/cm²	[pollutant] = 2.0 mM/L, [catalyst] = 0.8 g/L, pH = 9.5, temperature = 26 °C	80%; 300 min	Yang et al.[64]
paracetamol	ZnO NRs, ZnO-Ag NRs	simulated solar light (1000 W/m²)	[pollutant] = 20 ppm, [catalyst] = thin film	20%; 300 min 20%; 300 min	Al-Gharibi et al.[57]
paracetamol	TiO_2–P25 (commercial), TiEt400, TiPr400	UV lamp (150 W)	[pollutant] = 50 ppm, [catalyst] = 1.33 g/L, pH = 9, temperature = 25 °C	~30%; ~60%; ~50%; 180 min	Raquel et al.[58]
paracetamol	ZnO	compact fluorescent lamp (20 W)	[pollutant] = 100 ppm, [catalyst] = 10 g/L, temperature = 25 °C	<1%; 180 min	Thi et al.[68]
paracetamol	Fe_2O_3	medium pressure mercury vapor lamp (450W)	[pollutant] = 50 ppm, [catalyst] = 0.1 g/L	52.5%; 90 min	Abdel-Wahab et al.[69]
paracetamol	1.1% ZnO-PS (ZnO deposited on PS pellets)	UV-LED strip (14W/m), (365 nm)	[pollutant] = 12.5 ppm, [catalyst] = 25 g/L, pH = 6.5	70%; 240 min	Vaiano et al.[70]
paracetamol	CZnO–Pd nanofiber film coated on FTO	halogen lamp (150 W) (420–600 nm)	[pollutant] = 0.1 mM/L, $[Na_2SO_4]$ = 50 mM/L, pH = 7	71%; 180 min	Nada et al.[71]
paracetamol	ZnO nanoparticles; MI-ZnO nanoparticles	UV lamp (4 mW/cm²) (368 nm)	[pollutant] = 5×10^{-5} M, [catalyst] = 1.0 mg, pH = 7.2	20%; 180 min.; 86%; 180 min.	Cantarella et al.[15]

Table 8. Comparison of Removal Efficiencies without a Photocatalyst with Previous Studies

name of pollutant	photolysis	light source	experimental conditions	% removal/ exposure duration	references
PCM1	UV/H_2O_2	UV lamp (25 W) (280–400 nm)	[pollutant] = 20 ppm, $[H_2O_2]$ = 3 mL, temperature = 27 °C	no change; 180 min	our work
PCM2	UV/H_2O_2	UV lamp (25 W) (280–400 nm)	[pollutant] = 20 ppm, $[H_2O_2]$ = 3 mL, temperature = 27 °C	no change; 180 min	our work
paracetamol	UV/H_2O_2	UV lamp (254 nm)	[pollutant] = 4 mM/L, $[H_2O_2]$ = 48 mM/L, pH = 9, temperature = 26 °C	<5%; 360 min	Yang et al.[63]
paracetamol	UV	UV A (8 W) (365 nm)	[pollutant] = 4 mM/L, pH = 5.5, temperature = 26 °C	no change; 300 min	Yang et al.[64]
paracetamol	UV	UV C (15 W) (254 nm)	[pollutant] = 4 mM/L, pH = 5.3, temperature = 26 °C	~50%; 300 min	Yang et al.[64]
paracetamol	simulated solar light (1000 W/m²)	simulated solar light (1000 W/m²)	[pollutant] = 20 ppm	no change; 240 min	Al-Gharibi et al.[57]
paracetamol	UV	UV lamp (150 W)	[pollutant] = 50 ppm; pH = 9; temperature = 25 °C	no change; 120 min	Trujillano et al.[58]
paracetamol	UV	UV lamp (4 mW/cm²) (368 nm)	[pollutant] = 5×10^{-5} M; pH = 7.2	no change; 180 min	Cantarella et al.[15]

The percentage removal of the pollutant, paracetamol, obtained in the present work compares well with the previous studies, and in fact, in most of the cases, the performance of as-prepared ZnO sample 2 along with H_2O_2 is found to be better than the others mentioned in literature. Here, a huge quantity of the pollutant paracetamol has been successfully removed. Therefore, the use of ZnO sample 2 along with H_2O_2 proves to be a suitable technique for the removal of paracetamol from the polluted water. The photocatalyst ZnO sample 2 is highly stable for the generation of hydroxyl radicals and superoxide radical ions for the degradation of paracetamol, and thus reusability of ZnO NSs is ensured. For the sake of completeness, results for photolysis only, i.e., exposure of polluted water samples to UV+H_2O_2, without the presence of any photocatalyst, are summarized in Table 8 and also given in Figure S2, where it can be seen that hardly any degradation or removal takes place. In Figure S2, a curve of the experimental findings based on the role of H_2O_2 alone in the degradation of PCM1 without the presence of catalysts and UV light is also mentioned. These two experiments were performed to test the role of the ZnO sample 2 catalyst in the photocatalytic degradation of PCM1 and PCM2, which confirms that the observed changes are due to the combination ZnO+UV and ZnO+H_2O_2+UV.

4. CONCLUSIONS

In conclusion, ZnO samples 1 and 2 with a hexagonal wurtzite structure are successfully synthesized via the sol−gel method using concentrations of 3.17 and 4.17 M NaOH. The XRD result demonstrates that, in order to generate the maximum pure sample, the ideal NaOH concentration for ZnO synthesis is less than 4.17. The results of the experiment demonstrated that hydroxyl ions are crucial to the synthesis of ZnO samples. By increasing the concentration of NaOH to 4.17, a red shift is observed in the UV−vis absorbance peak of ZnO samples. When the concentration of NaOH is increased from 3.17 to 4.17 M, the optical band gap energy of ZnO samples shifts from 3.33 to 3.01 eV for sample 1 and sample 2, respectively. With a higher concentration of NaOH, the growth of the crystallite size causes a slight shift in the band gap. It has been confirmed that using a NaOH concentration of 4.17 M or higher is not a suitable solution for producing a high-purity ZnO sample. However, the impure ZnO sample 2 will become the future catalyst due to the presence of zincate ion, because it is environmentally friendly, is applied in the health industry, and will also help in the degradation reaction of paracetamol. An 83% (67%) removal of PCM1 (PCM2) for 20 ppm pollutant was achieved using the UV/H_2O_2 reaction system in 180 min of duration. The highest reaction rate constant of 0.0097 among all the reactions is found for the removal of PCM1 in the UV/H_2O_2 reaction system. H_2O_2 as expected accelerates the production of hydroxyl radicals, which in turn accelerates the degradation of paracetamol and shows very good cleaning results. The half-life of PCM1 here is 71.5 min, or in other words, the pollutant quantity of 10 mg/L is removed in 71.5 min, which is a remarkably good number as compared to reported results. The percentage removal of PCM1 and PCM2, using as-prepared ZnO sample 2 in the UV/H_2O_2 reaction system, obtained in the present work compares favorably well with the previously reported literatures. Therefore, the use of ZnO NSs along with H_2O_2 can be a suitable technique for the removal of paracetamol from polluted water. The mineralization of paracetamol is in agreement with the pseudo-first-order model. However, the removal of PCM2 by ZnO sample 2 is strongly dominated by the pseudo-second-order kinetic model.

The removal capacity of the as-prepared ZnO NSs at equilibrium is close to the pseudo-second-order kinetic model for the removal of both types of paracetamol. The photocatalyst ZnO NSs can be reused for cleaning water at least four times. The degradation in absence of ZnO is nil, or in other words, a simple photolysis does not work. Thus, UV photocatalysis in the presence of ZnO NSs and H_2O_2 in a mildly acidic environment is a promising technique for removal of paracetamol—a menace especially in the Covid-19 scenario from water. There was no peak present at 243 nm of PCM1 with UV/H_2O_2. Hence the 100% successful conversion of 20 ppm of PCM1 in the presence of the as-prepared ZnO sample 2 catalyst in the UV/H_2O_2 reaction system. This study is regarded as an inexpensive, environmentally friendly way of improving ZnO NSs' photocatalytic activity in the UV−vis region and also for possible application in highly effective solar energy conversion devices by the use of dye sensitization.

■ ASSOCIATED CONTENT

ⓈⒾ Supporting Information

The Supporting Information is available free of charge at https://pubs.acs.org/doi/10.1021/acsomega.4c06272.

A comparative XRD pattern of as-synthesizd ZnO sample 2 and zinc acetate; experimental setup for the photocatalytic degradation-based photoreactor system in both UV and UV/H_2O_2 reaction systems; effect of H_2O_2 alone and H_2O_2 + UV light exposure on the photocatalytic degradation; scavenging activity test using isopropanol to identify the active radical species; and EC-MS spectra for photocatalytic degradation of PCM1 and PCM2 using ZnO sample 2 in both UV and UV/H_2O_2 reaction systems (PDF)

■ AUTHOR INFORMATION

Corresponding Author

Sharda Pandey − *Department of Physics, University of Lucknow, Lucknow, U.P. 226007, India;* ⊙ orcid.org/0000-0001-9950-1195; Email: sharda2012536@gmail.com

Authors

Anchal Srivastava − *Department of Physics, University of Lucknow, Lucknow, U.P. 226007, India*

Poonam Rawat − *Department of Chemistry, University of Lucknow, Lucknow, U.P. 226007, India*

Satendra Kumar Chauhan − *Department of Physics, University of Lucknow, Lucknow, U.P. 226007, India*

Anant Ram − *Department of Chemistry, University of Lucknow, Lucknow, U.P. 226007, India*

Vishnu Kumar Diwedi − *Department of Physics, University of Lucknow, Lucknow, U.P. 226007, India*

Rajesh Kumar Shukla − *Department of Physics, University of Lucknow, Lucknow, U.P. 226007, India*

Navina Wadhwani − *Department of Physics, University of Lucknow, Lucknow, U.P. 226007, India*

Complete contact information is available at:
https://pubs.acs.org/10.1021/acsomega.4c06272

Notes

The authors declare no competing financial interest.

■ REFERENCES

(1) de la Cruz, N.; Giménez, J.; Esplugas, S.; Grandjean, D.; De Alencastro, L. F.; Pulgarín, C. Degradation of 32 emergent contaminants by UV and neutral photo-fenton in domestic wastewater effluent previously treated by activated sludge. *Water Res.* **2012**, *46*, 1947−1957.

(2) Oller, I.; Malato, S.; Sánchez-Pérez, J. A. Combination of advanced oxidation processes and biological treatments for wastewater decontamination—A review. *Sci. Total Environ.* **2011**, *409*, 4141−4166.

(3) De la Cruz, N.; Dantas, R. F.; Giménez, J.; Esplugas, S. Photolysis and TiO2 photocatalysis of the pharmaceutical propranolol: Solar and artificial light. *Appl. Catal., B* **2013**, *130−131*, 249−256.

(4) Fick, J.; Söderström, H.; Lindberg, R. H.; Phan, C.; Tysklind, M.; Larsson, D. G. J. Contamination of surface, ground, and drinking water from pharmaceutical production. *Environ. Toxicol. Chem.* **2009**, *28*, 2522.

(5) Skoczko, I.; Piekutin, J. Photo-Fenton method usage to organic compounds degradation. *Desalin. Water Treat.* **2014**, *52*, 3837−3842.

(6) Mompelat, S.; Le Bot, B.; Thomas, O. Occurrence and fate of pharmaceutical products and by-products, from resource to drinking water. *Environ. Int.* **2009**, *35*, 803−814.

(7) Serpone, N.; Artemev, Y. M.; Ryabchuk, V. K.; Emeline, A. V.; Horikoshi, S. Light-driven advanced oxidation processes in the disposal of emerging pharmaceutical contaminants in aqueous media: a brief review. *Curr. Opin. In Green Sustain. Chem.* **2017**, *6*, 18−33.

(8) https://www.astrazeneca.com/sustainability/environmental-protection/pharmaceuticals-in-the-environment.html.

(9) https://www.astrazeneca.com/content/dam/az/PDF/2018/A2E303_Pharmaceutical%20in%20the%20environment_A4_Final_V4.pdf.

(10) Ebele, A. J.; Abdallah, M. A. E.; Harrad, S. Pharmaceuticals and personal care products (PPCPs) in the fresh water aquatic environment. *Emerging Contam.* **2017**, *3*, 1−16.

(11) Yang, Y.; Ok, Y. S.; Kim, K. H.; Kwon, E. E.; Tsang, Y. F. Occurrences and removal of pharmaceuticals and personal care products(PPCPs) in drinking water and water/sewage treatment plants: a review. *Sci. Total Environ.* **2017**, *596−597*, 303−320.

(12) Patel, M.; Kumar, R.; Kishor, K.; Mlsna, T.; Pittman, C. U.; Mohan, D. Pharmaceuticals of Emerging Concern in Aquatic Systems: Chemistry, Occurrence, Effects, and Removal Methods. *s: Chem. Rev.* **2019**, *119*, 3510−3673.

(13) Gangishetty, S.; Verma, S. RP-HPLC method development and validation for simultaneous estimation of clarithromycin and paracetamol. *ISRN Anal Chem.* **2013**, *2013*, 1−5.

(14) EC *Technical guidance document in support of commission directive 93/67/EEC on risk assessment for new notified substances and commission*; 2003.

(15) Cantarella, M.; Di Mauro, A.; Gulino, A.; Spitaleri, L.; Nicotra, G.; Privitera, V.; Impellizzeri, G. Selective photodegradation of paracetamol by molecularly imprinted ZnOnanonuts. *Applied Catalysis B: Environmental.* **2018**, *238*, 509−517.

(16) Moctezuma, E.; Leyva, E.; Aguilar, C. A.; Luna, R. A.; Montalvo, C. Photocatalytic degradation of paracetamol: Intermediates and total reaction mechanism. *J. of Haz. Mate.* **2012**, *243*, 130−138. ISSN 0304−3894.

(17) Oturan, M. A.; Aaron, J. J. Advanced oxidation processes in water/wastewater treatment: Principles and applications. A review. *Crit. Rev. Environ. Sci. Technol.* **2014**, *44*, 2577−2641.

(18) El Kateb, M.; Trellu, C.; Darwich, A.; Rivallin, M.; Bechelany, M.; Nagarajan, S.; Lacour, S.; Bellakhal, N.; Lesage, G.; Héran, M.; Cretin, M. Electrochemical advanced oxidation processes using novel electrode materials for mineralization and biodegradability enhancement of nanofiltration concentrate of landfill leachates. *Water Res.* **2019**, *162*, 446−455.

(19) Pirhashemi, M.; Habibi-Yangjeh, A.; RahimPouran, S. Review on the criteria anticipated for the fabrication of highly efficient ZnO-based visible-light-driven photocatalysts. *J. Ind. Eng. Chem.* **2018**, *62*, 1−25.

(20) Rai, R. S.; P, G. J.; Bajpai, V.; Khan, M. I.; Elboughdiri, N.; Shanableh, A.; Luque, R. An eco-friendly approach on green synthesis, bio-engineering applications, and future outlook of ZnO nanomaterial: A critical review. *Environ. Res.* **2023**, *221*, No. 114807.

(21) Malik, S.; Muhammad, K.; Waheed, Y. Nanotechnology: a revolution in modern industry. *Molecules.* **2023**, *28*, 661.

(22) Singh, J.; Dutta, T.; Kim, K. H.; et al. Green synthesis of metals and their oxide nanoparticles: applications for environmental remediation. *J. Nanobiotechnology.* **2018**, *16*, 1.

(23) Wei, Z.; Dabodiya, T. S.; Chen, J.; Lu, Q.; Qian, J.; Meng, J.; Zeng, H.; Qian, H.; Zhang, X. In-situ fabrication of metal oxide nanocaps based on biphasic reactions with surface nanodroplets. *J. Colloid Interface Sci.* **2022**, *608*, 2235−2245.

(24) Gatoo, M. A.; Naseem, S.; Arfat, M. Y.; Mahmood Dar, A.; Qasim, K.; Zubair, S. Physicochemical Properties of Nanomaterials: Implication in Associated Toxic Manifestations. *BioMed. Research International.* **2014**, *2014*, 1−8.

(25) Gavrilenko, E. A.; Goncharova, D. A.; Lapin, I. N.; Nemoykina, A. L.; Svetlichnyi, V. A.; Aljulaih, A. A.; Mintcheva, N.; Kulinich, S. A. Comparative Study of Physicochemical and Antibacterial Properties of ZnO Nanoparticles Prepared by Laser Ablation of Zn Target in Water and Air. *Materials* **2019**, *12* (1), 186.

(26) Venkataprasad Bhat, S.; Govindaraj, A.; Rao, C. N. R. Hybrid solar cell based on P3HT−ZnO nanoparticle blend in the inverted device configuration. *Solar Energy Materials & Solar Cells.* **2011**, *95*, 2318.

(27) Xu, C.; Yang, C.; Gu, B.; Fang, S. Nanostructured ZnO for biosensing applications. *Chin. Sci. Bull.* **2013**, *58*, 2563.

(28) Katiyar, A.; Kumar, N.; Shukla, R. K.; Srivastava, A. Influence of alkali hydroxides on synthesis, physico-chemical and photoluminescence properties of zinc oxide nanoparticles. *Mater. Today: Proc.* **2020**, *29*, 885.

(29) Umar, A.; Chauhan, M. S.; Chauhan, S.; Kumar, R.; Kumar, G.; Al-Sayari, S. A.; Hwang, S. W.; Al-Hajry, A. Large-scale synthesis of ZnO balls made of fluffy thin nanosheets by simple solution process: Structural, optical and photocatalytic properties. *J. Colloid Interface Sci.* **2011**, *363*, 521−528.

(30) Barka-Bouaifel, F.; Sieber, B.; Bezzi, N.; Benner, J.; Roussel, P.; Boussekey, L.; Szunerits, S.; Boukherroub, R. Synthesis and photocatalytic activity of iodine-doped ZnO nanoflowers. *J. of Mater. Chem.* **2011**, *21*, 10982−10989.

(31) Sachin; Jaishree; Singh, N.; et al. Green synthesis of zinc oxide nanoparticles using lychee peel and its application in anti-bacterial properties and CR dye removal from wastewater. *Chemosphere* **2023**, *327*, No. 138497.

(32) Vasantharaj, S.; Sathiyavimal, S.; Senthilkumar, P.; Kalpana, V. N.; Rajalakshmi, G.; Alsehli, M.; Elfasakhany, A.; Pugazhendhi, A. Enhanced photocatalytic degradation of water pollutants using bio-green synthesis of zinc oxide nanoparticles (ZnO NPs). *J. of Envir. Chem. Eng.* **2021**, *9*, No. 105772.

(33) Despotović, V.; Finčur, N.; Bognar, S.; Šojić Merkulov, D.; Putnik, P.; Abramović, B.; Panić, S. Characterization and Photocatalytic Performance of Newly Synthesized ZnO Nanoparticles for Environmental Organic Pollutants Removal from Water System. *Separations* **2023**, *10*, 258.

(34) Sultana, K. A.; Islam, Md. T.; Silva, J. A.; Turley, R. S.; Hernandez-Viezcas, J. A.; Gardea-Torresdey, J. L.; Noveron, J. C. Sustainable synthesis of zinc oxide nanoparticles for photocatalytic degradation of organic pollutant and generation of hydroxyl radical. *J. Mol. Liq.* **2020**, *307*, No. 112931.

(35) Park, J. H.; Park, C.; Lee, K. S.; Suh, S. J. Effect of NaOH and precursor concentration on size and magnetic properties of FeCo nanoparticles synthesized using the polyol method. *AIP Advances* **2020**, *10*, 115220.

(36) Golić, D. L.; Branković, G.; Nešić, M. P.; Vojisavljević, K.; Rečnik, A.; Daneu, N.; Bernik, S.; Šćepanović, M.; Poleti, D.; Branković, Z. Structural characterization of self-assembled ZnO nanoparticles obtained by the sol−gel method from Zn-(CH3COO)2·2H2O. *Nanotechnology* **2011**, *22*, No. 395603.

(37) Katiyar, A.; Kumar, N.; Shukla, R. K.; Srivastava, A. Growth and study of c-axis-oriented vertically aligned ZnOnanorods on seeded substrate. *J. Mater. Sci: Mater. Electron.* **2021**, *32*, 15687−15706.

(38) Mamat, M. H.; Khusaimi, Z.; Musa, M. Z.; Sahdan, M. Z.; Rusop, M. Novel synthesis of aligned Zinc oxide nanorods on a glass

substrate by sonicated sol−gel immersion. *Mater. Lett.* **2010**, *64*, 1211−1214.

(39) Hassan, M. M.; Khan, W.; Azam, A.; Naqvi, A. H. Effect of size reduction on structural and optical properties of ZnO matrix due to successive doping of Fe ions. *J. of Lumi.* **2014**, *145*, 160−166.

(40) Zarnaghash, N.; Rezaei, R.; Hayati, P.; Moaser, A. G.; Doroodmand, M. M. Shape-controlled synthesis of sodium zincate mesoporous structures based on sulfonated melamine formaldehyde and their application as catalysts for Biginelli reaction. *J. Mol. Struct.* **2021**, *1232*, No. 130028.

(41) Ashfold, M. N.; Doherty, R. P.; Ndifor-Angwafor, N. G.; Riley, D. J.; Sun, Y. The kinetics of the hydrothermal growth of ZnO nanostructures. *Thin Solid Films.* **2007**, *515*, 8679−8683.

(42) Zeng, Q.; Xue, S.; Wu, S.; Gan, K.; Xu, L.; Han, J.; Zhou, W.; Zou, R. Synthesis and characterization of ZnSe rose-like nanoflowers and microspheres by the hydrothermal method. *Ceram. Int.* **2014**, *40*, 2847−2852.

(43) Srivastava, A.; Kumar, N.; Khare, S. Enhancement in UVemission and band gap by Fe doping in ZnO thin films. *Opto-Electron. Rev.* **2014**, *22*, 68−76.

(44) Pandey, S.; Chauhan, S. K.; Shukla, R. K.; Srivastava, A. Systematic Investigation of Structural, Morphological and Optical Properties of Fe Doped ZnO Nanorods and Its Nanocomposite with Graphite Oxide. *J. Mater. Eng. Perform.* **2024**, 1−20.

(45) Zak, A. K.; Majid, W. H. A.; Abrishami, M. E.; Yousefi, R. X-ray analysis of ZnO nanoparticles by Williamson−Hall and size−strain plot methods. *Solid State Sci.* **2011**, *13*, 251−256.

(46) Koutu, V.; Shastri, L.; Malik, M. M. Effect of NaOH concentration on optical properties of zinc oxide nanoparticles. *Mater. Sci.-Pol.* **2016**, *34*, 819.

(47) Xu, S.; Wang, Z. L. One-dimensional ZnO nanostructures: Solution growth and functional properties. *Nano Res.* **2011**, *4*, 1013−1098.

(48) Ren, F.; Xin, R.; Ge, X.; Leng, Y. Characterization and structural analysis of zinc-substituted hydroxyapatites. *Acta Biomater.* **2009**, *5*, 3141−3149.

(49) Williamson, G. K.; Hall, W. H. X-ray line broadening from filed aluminium and wolfram. *Acta. Metall.* **1953**, *1*, 22−31.

(50) Wahab, H. A.; Salama, A. A.; et al. Optical, structural and morphological studies of ZnO nano-rod thin films for biosensor applications using sol-gel. *Res. In Phys.* **2013**, *3*, 46−51.

(51) Chai, C. The Global Market for Zinc Oxide Nanopowders. *N. Rep. Global Zinc Oxide Nanopowder Mark.* **2012**, 135−140.

(52) Tseng, Y. K.; Chuang, M. H.; Chen, Y. C.; Wu, C. H. Synthesis of 1D, 2D and 3D ZnO Polycrystalline Nanostructures Using Sol-Gel Method. *Journal of Nanotechnology* **2012**, *2012*, 1−8.

(53) Bari, A. R.; Shinde, M. D.; Deo, V.; Patil, L. A. Effect of Solvents on the Particle Morphology of nanostructured ZnO. *Ind. J. Pure Appl. Phys.* **2009**, *47*, 24−27.

(54) Pandey, S.; Rawat, P.; Ram, A.; Chauhan, S. K.; Singh, R. N.; Shukla, R. K.; Srivastava, A. The mechanistic pathway of paracetamol degradation using UV/H2O2 with PVP functionalized ZnO Nanorods. *J. Mol. Struct.* **2024**, *1317*, No. 139068.

(55) Idiawati, R.; Mufti, N.; Taufiq, A.; Wisodo, H.; Laila, I. K. R.; Fuad, A.; Sunaryono. Effect of Growth Time on the Characteristics of ZnO Nanorods. *IOP Conf. Ser.: Mater. Sci. Eng.* **2017**, *202*, No. 012050.

(56) Pronin, I. A.; Kaneva, N. V.; Bozhinova, A. S.; Averin, I. A.; Papazova, K. I.; Dimitrov, D. Ts.; Moshnikov, V. A. Photocatalytic Oxidation of Pharmaceticals on Thin Nanostructured Zinc Oxide Films. *Kin. and Catal.* **2014**, *55*, 167−171.

(57) Al-Gharibi, M. A.; Kyaw, H. H.; Al-Sabahi, J. N.; Myint, M. T. Z.; Al-Sharji, Z. A.; Al-Abri, M. Z. Silver nanoparticles decorated zinc oxide nanorods supported catalyst for photocatalytic degradation of paracetamol. *Mater. Sci. Semicond. Process.* **2021**, *134*, No. 105994.

(58) Trujillano, R.; Rives, V.; García, I. Photocatalytic Degradation of Paracetamol in Aqueous Medium Using TiO2 Prepared by the Sol−Gel Method. *Molecules.* **2022**, *27*, 2904.

(59) Sheela, T.; Nayaka, Y. A.; Viswanatha, R.; Basavanna, S.; Venkatesha, T. G. Kinetics and thermodynamics studies on the adsorption of Zn(II), Cd(II), and Hg(II) from aqueous solution using Zinc Oxide nanoparticles. *Powder Technol.* **2012**, *217*, 163−170.

(60) Daneshvar, N.; Salari, D.; Khataee, A. R. Photocatalytic degradation of azo dye acid red 14 in water on ZnO as an alternative catalyst to TiO_2. *J. of Photochem. and Photobio. A: Chem.* **2004**, *162*, 317−322.

(61) Xu, Y.; Schoonen, M. A. A. The absolute energy positions of conduction and valence bands of selected semiconducting minerals. *Am. Mineral.* **2000**, *85*, 543−556.

(62) Armstrong, D. A.; Huie, R. E.; Koppenol, W. H.; Lymar, S. V.; Merényi, G.; Neta, P.; Ruscic, B.; Stanbury, D. M.; Steenken, S.; Wardman, P. Standard electrode potentials involving radicals in aqueous solution: inorganic radicals (IUPAC Technical Report). *Pure Appl. Chem.* **2015**, *87*, 1139−1150.

(63) YANG, L.; YU, L. E.; RAY, M. B. Photocatalytic Oxidation of Paracetamol: Dominant Reactants, Intermediates, and Reaction Mechanisms. *Environ. Sci. Technol.* **2009**, *43*, 460−465. *A.C.S. Published on Web 12/15/2008.*

(64) Yang, L.; Yu, L. E.; Ray, M. B. Degradation of paracetamol in aqueous solutions by TiO_2 photocatalysis. *Water Res.* **2008**, *42*, 3480−3488.

(65) Ho, Y. S.; McKay, G. Pseudo-second order model for sorption processes. *Process Biochem.* **1999**, *34* (5), 451−465.

(66) Revellame, E. D.; Fortela, D. L.; Sharp, W.; Hernandez, R.; Zappi, M. E. Adsorption kinetic modeling using pseudo-first order and pseudo-second order rate laws: A review. *Cleaner Enginee. and Technol.* **2020**, *1*, No. 100032.

(67) Elbadawy, H. A.; Elhusseiny, A. F.; Hussein, S. M.; et al. Sustainable and energy-efficient photocatalytic degradation of textile dye assisted by ecofriendly synthesized silver nanoparticles. *Sci. Rep.* **2023**, *13*, 2302.

(68) Thi, V.H.-T.; Lee, B.-K. Effective photocatalytic degradation of paracetamol using La-doped ZnOphotocatalyst under visible light irradiation. *Mate. Res. Bulle.* **2017**, *96*, 171−182.

(69) Abdel-Wahab, A.-M.; Al-Shirbini, A.-S.; Mohamed, O.; Nasr, O. Photocatalyticdegradation of paracetamol over magnetic flower-like TiO_2 /Fe_2O_3 core-shell nanostructures. *J. of Photochem. and Photobio. A: Chem.* **2017**, *347*, 186−198.

(70) Vaiano, V.; Matarangolo, M.; Sacco, O. UV-LEDs floating-bed photoreactor for the removal of caffeine and paracetamol using ZnO supported on polystyrene pellets. *Chem. Eng. J.* **2018**, *350*, 703.

(71) Nada, A. A.; Orimolade, B. O.; El-Maghrabi, H. H.; Koiki, B. A.; Rivallin, M.; Bekheet, M. F.; Viter, R.; Damberga, D.; Lesage, G.; Iatsunskyi, I.; Coy, E.; Cretin, M.; Arotiba, O. A.; Bechelany, M. Photoelectrocatalysis of paracetamol on Pd−ZnO/N-doped carbon nanofibers electrode. *Appl. Mater. Today* **2021**, *24*, No. 101129.